Neutrinos from the milky way

Visser, E.L.

4

SIMULATION, TRIGGERS AND RECONSTRUCTION

In this chapter the triggering of the data that are sent to shore and the subsequent reconstruction of the neutrino interaction from these triggered data are described.

Before going into triggers and reconstruction, the simulation packages used to simulate the response of the detector to neutrino interactions and muons are described in section 4.1. These simulations are needed to quantify the performance of the trigger algorithms and reconstruction strategies.

In section 4.2 the trigger scheme and the different triggers used in the ANTARES detector are described. In section 4.3 the reconstruction of the neutrino direction and energy determination are described. The part on reconstruction is focused on the so-called *track reconstruction*, which is used to determine the direction of the muon produced in a CC muon-neutrino interaction. Several algorithms are used within the ANTARES collaboration, which are described together with a new track reconstruction algorithm, called GRIDFIT. The goal of this new algorithm is to improve the reconstruction efficiency for low energy neutrinos.

4.1 SIMULATION TOOLS

The simulation chain used in ANTARES consists of several steps. First neutrinos and atmospheric muons are generated using the GENHEN [L'Abbate et al., 2004] and MUPAGE [Carminati et al., 2008] packages respectively. Then, the charged particles are propagated through the detector using the KM3 [Navas and Thompson, 1999] and GEASIM [Brunner, 2002] packages. Finally the detector response to the Čerenkov light is simulated using the TRIGGER-EFFICIENCY [de Jong, 2010] program. These different steps are described in more detail below.

4.1.1 *Neutrino generation*

The rate of neutrinos detected by a detector can be written as [Bailey, 2002]:

$$R = \int\int\int \mathrm{d}E_\nu \, \mathrm{d}\Omega \, \mathrm{d}\vec{x} \, \Phi_\nu(E_\nu, \theta, \phi) \, \rho(\vec{x}) \, N_\mathrm{A} \, \sigma_{\nu\mathrm{N}}(E_\nu) \cdot P_\mathrm{det}(E_\nu, \theta, \phi, \vec{x}) \, P_\oplus(E_\nu, \theta, \phi), \tag{4.1}$$

where Ω is the solid angle, $\vec{x}$ is the position of the neutrino interaction, θ and ϕ are the zenith and azimuth angle in local detector coordinates respectively, $\Phi_\nu(E_\nu, \theta, \phi)$ is the neutrino flux at the surface of the Earth, $\rho(\vec{x})$ is the density of the medium in which the neutrino interacts and N_A is Avogadro's constant.

Furthermore, there are two probability terms in equation 4.1. The first, $P_\mathrm{det}(E_\nu, \theta, \phi, \vec{x})$, represents the probability that the neutrino interaction is detected. This depends on a number of factors, such as the location of the interaction, the amount of light produced by the interaction products, the detector response and the trigger and reconstruction efficiencies. The other probability term, $P_\oplus(E_\nu, \theta, \phi)$, represents the probability for the neutrino to penetrate the Earth, and is given by:

$$P_\oplus(E_\nu, \theta, \phi) = e^{-N_\oplus(\theta,\phi) N_\mathrm{A} \sigma_{\nu\mathrm{N}}(E_\nu)}, \tag{4.2}$$

with

$$N_\oplus(\theta, \phi) = \int \mathrm{d}s \, \rho_\oplus(s), \tag{4.3}$$

the mass density per unit of area integrated along a line of sight through the Earth as seen from the detector (i. e. the column density), with s the integration variable and $\rho_\oplus(s)$ the matter density of the Earth.

GENHEN: GENerator of High Energy Neutrinos

Neutrino events are generated with the GENHEN package. For this purpose, a large cylinder is defined around the detector in which neutrino events are generated isotropically. The size of this cylinder is chosen in such a way that all neutrinos that are able to produce a detectable signal in the detector are simulated. It has a typical radius and height of 25 km.

A second cylinder, called the *can* is defined, and only events that either have their vertex inside of this can (for CC electron-neutrino and NC interactions) or have a muon or tau reaching the can (for CC muon- and tau-neutrino interactions) are taken into account. Events for which the muon (or tau) direction is such that it does not intercept the can are discarded. The can typically

extends 3 light attenuation lengths beyond the instrumented volume and muons passing outside of it are too far away to produce a detectable signal in the PMTs. Typical values for the radius and height of the can are 300 m and 650 m respectively. The CTEQ6-DIS parton distribution functions [Pumplin et al., 2002] are used to calculate the cross sections and the Preliminary Reference Earth Model [Dziewonski and Anderson, 1981] is used to calculate the neutrino attenuation in the Earth.

To evaluate the triple integral in equation 4.1, GENHEN makes use of Monte Carlo (MC) integration[18], which is a mathematical technique in which an integral is approximated by evaluating the integrand at a number of randomly chosen points in the phase space. Equation 4.1 can then be written as:

$$R = \frac{V_{\text{gen}} I_\phi I_\theta I_E}{N_{\text{gen}}} \sum_{i=1}^{N_{\text{gen}}} \Phi_\nu(E_{\nu,i}, \theta_i, \phi_i)\, \rho(\vec{x}_i)\, N_A\, \sigma_{\nu N}(E_{\nu,i}) \cdot P_\oplus(E_{\nu,i}, \theta_i, \phi_i)\, P_{\text{det,i}}\, E_{\nu,i}^{\alpha}, \tag{4.4}$$

where V_{gen} is the generation volume, N_{gen} the number of generated events (typically of the order of 10^{10}) and α the spectral index of the generation spectrum. The events are generally not generated uniformly in the neutrino energy (i. e. $\alpha = 0$), but rather according to a power law spectrum. This is done to generate roughly the same number of events for each decade of neutrino energy. The value of α is typically around 1.4.

The three phase space factors I_ϕ, I_θ and I_E in equation 4.4 are given by:

$$I_\phi = \int_{\phi_{\min}}^{\phi_{\max}} \mathrm{d}\phi = \phi_{\max} - \phi_{\min}, \tag{4.5}$$

$$I_\theta = \int_{\theta_{\min}}^{\theta_{\max}} \mathrm{d}\theta\ \sin\theta = \cos(\theta_{\min}) - \cos(\theta_{\max}), \tag{4.6}$$

$$I_E = \int_{E_{\nu,\min}}^{E_{\nu,\max}} \mathrm{d}E_\nu\ E_\nu^{-\alpha} = \begin{cases} \frac{E_{\nu,\max}^{1-\alpha} - E_{\nu,\min}^{1-\alpha}}{1-\alpha} & \alpha \neq 1 \\ \ln \frac{E_{\nu,\max}}{E_{\nu,\min}} & \alpha = 1 \end{cases} \tag{4.7}$$

Finally, the term representing the probability that the neutrino interaction is detected ($P_{\text{det,i}}$ in equation 4.4) is now a binary variable, which is 1 if the event is triggered, reconstructed, etc. and 0 if not.

[18] *The method is named by physicist John von Neumann (*1903; †1957), who worked together with Stanislaw Ulam (*1909; †1984) on the Manhattan Project, where the technique was used. Since the project was secret, a code name was required and Von Neumann chose the name Monte Carlo, after the Monte Carlo casino in Monaco where Ulam's uncle used to gamble.*

By defining the so-called *event weight*, which captures the whole interaction and detection process:

$$w_i \equiv V_{\text{gen}}\, I_\Phi\, I_\theta\, I_E\, \rho(\vec{x}_i)\, N_A\, \sigma_{\nu N}(E_{\nu,i})\, P_\oplus(E_{\nu,i},\, \theta_i,\, \phi_i)\, P_{\text{det,i}}\, E_{\nu,i}^{\alpha}, \tag{4.8}$$

equation 4.4 can be written as:

$$R = \frac{1}{N_{\text{gen}}} \sum_{i=1}^{N_{\text{gen}}} w_i\, \Phi_\nu(E_{\nu,i},\, \theta_i,\, \phi_i), \tag{4.9}$$

and event rates for different neutrino fluxes can easily be calculated by multiplying the event weight by the required flux on an event by event basis.

4.1.2 *Atmospheric muon generation*

MUPAGE: atmospheric MUons from PArametric formulas: a fast GEnerator for neutrino telescopes

Atmospheric muon events are generated using the MUPAGE package. Instead of using a full MC simulation as for the neutrino generation, MUPAGE uses a set of parametric formulas to reproduce the energy and angular distribution of muon bundles of any multiplicity (typically up to 100) on the surface of the can. For MUPAGE the generated number of events corresponds to the livetime specified by the user.

4.1.3 *Propagation of muons, light and other secondaries*

The muons are propagated through the can using the KM3 package, which simulates the energy losses of the muon and generates photons along the muon track. The created photons are also propagated through the sea water, taking into account both absorption and scattering. Since tracking all photons is too computationally intensive, tables are used that contain the average number of photons arriving at a PMT with a given orientation and at a given distance from the muon track.

GEANT: GEometry ANd Tracking

All other particles are propagated using the GEASIM package, which is based on the GEANT package [Agostinelli, 2003] and performs a full tracking of all particles. Light scattering is not considered in GEASIM, and for this reason a new version of KM3 has recently been created, which performs the light creation and propagation for all particles [James, 2012].

4.1.4 *Detector simulation*

The final step involves the simulation of the detector response to the photons arriving at the PMTs. For this the TRIGGEREFFICIENCY program is used. This program simulates the response of the PMTs and the data acquisition system, and also adds optical background (see section 3.2.1).

The true number of signal photons is used to determine the integrated hit charge, which is smeared according to a Gaussian distribution with $\sigma = 0.3$ p.e. The time of the hit is smeared using a Gaussian with a width given by the TTS.

In addition to these signal hits, noise hits are added. These hits are generated according to a Poisson distribution, using the observed background rate of each PMT. After-pulses[19] are also added at this point. The charges of the background hits are generated according to the observed distributions of after-pulses and normal background hits.

The output at this stage is compatible with what is sent to shore by the detector and to which the trigger algorithms are applied, see section 4.2. These triggers are also simulated by the TRIGGEREFFICIENCY program.

[19] *There is a finite probability that a signal (or background) pulse is followed by a second pulse (called after-pulse), which is caused by the ionisation of residual gas in the PMT.*

4.1.5 *MC productions*

For the physics analyses, the so-called run-by-run (RBR) simulation has been developed [Riviére, 2012]. In this simulation, separate MC files are generated for each data run, and the observed background rates and detector conditions (such as which PMTs are operational and which triggers are active) are used. The software versions used for the RBR simulation are summarised in table 4.1. Muon bundles with multiplicities between 1 and 200 are simulated with MUPAGE, with the livetime of the simulation limited to one-third of the duration of the data run for computational reasons.

Since the rates and detector conditions vary in the RBR simulation, it is not well suited for the development of new reconstruction strategies, or for the comparison of two different ones. For these kinds of studies, a well defined background rate and a nominal detector are better suited. For this reason, a dedicated MC production is made (called fixed-conditions (FXC) simulation), with a fully working detector and the background rate fixed at 60 kHz. This production is used in the rest of this chapter. Slightly different versions of the MC programs are used than for the RBR simulation, as can be seen from table 4.1. In the FXC

PROGRAM	RBR VERSION	FXC VERSION
GENHEN	v6r10	v6r9
MUPAGE	v3r5	v3r4
KM3	v4r2	v4r4
GEASIM	v4r13	v4r13
TRIGGEREFFICIENCY	v2011-12-19	v2011-12-19

Table 4.1: The MC software versions used in the run-by-run (RBR) and fixed-conditions (FXC) simulations.

simulation, muon bundles with multiplicities up to 1000 are simulated with MUPAGE and only upgoing neutrino events ($\theta > 90^\circ$) are considered.

4.2 TRIGGERING

All PMT signals passing the ARS threshold of 0.3 p.e. are digitised and all digital data are sent to shore. These data are referred to as L0 hits and are used as input for the trigger algorithms running on the PCs in the shore station. Most of these hits are due to background however, so a pre-trigger is applied to reduce the input for the trigger algorithms [de Jong, 2005]. Hereby it is used that the optical background hits are uncorrelated and have primarily a charge equivalent to 1 p.e. To this end, hits on different PMTs on the same storey within 20 ns or hits with a high charge (typically above 3 p.e.) are selected. These hits are called L1 hits and are used as input for the different trigger algorithms.

The default run setup consists of using both the so-called 3N and 2T3 triggers, and the data taken with this run setup corresponds to what is used in most data analyses. When data taking conditions are favourable the so-called TQ trigger is also enabled, which has an improved efficiency for low energy neutrinos. These trigger algorithms are described first, after which the advantage of including TQ triggered events is assessed. Only a general overview will be given of the various trigger algorithms, for a more in depth description see the master thesis of Bakker [2011].

4.2.1 *The 3N trigger algorithm*

The general purpose ("standard") muon trigger is called the 3N trigger, which uses the fact that photons originating from the same muon are causally related in space and time.

When no muon direction is assumed, the causality criterion reads:

$$|t_i - t_j| \leqslant r_{ij} \frac{n_g}{c}, \tag{4.10}$$

where t_i and t_j are the times of a hit on PMT i and j respectively, n_g is the group refractive index and r_{ij} is the distance between PMT i and j.

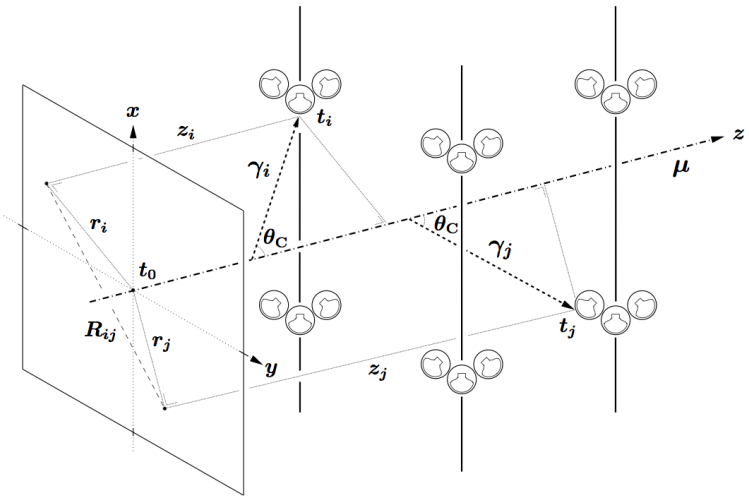

Figure 4.1: Schematic view of a muon traversing the ANTARES detector. Figure reproduced from Lim [2011].

When a muon direction is known, the causality criterion can be made more stringent. This can be seen from figure 4.1 in which the muon is chosen to travel along the z-axis. The time of a hit on PMT i can then be written as:

$$t_i = t_0 + \frac{1}{c}\left(z_i - \frac{r_i}{\tan(\theta_c)}\right) + \frac{n_g}{c}\frac{r_i}{\sin(\theta_c)}, \tag{4.11}$$

where t_0 is defined as the time when the muon is at $z = 0$, z_i is the position of PMT i along the muon track and r_i is the distance of closest approach of the muon to PMT i.

The difference in hit times of PMT i and PMT j can then be written as:

$$t_i - t_j = \frac{z_i - z_j}{c} + \frac{r_i - r_j}{c}\left(n_g \frac{1}{\sin(\theta_c)} - \frac{1}{\tan(\theta_c)}\right), \quad (4.12)$$

$$= \frac{z_i - z_j}{c} + \frac{r_i - r_j}{c}\tan(\theta_c), \quad (4.13)$$

where in the second step it has been assumed that $n_g = n$.

When the direction of the muon is assumed, the position of the track relative to PMTs i and j is still free. The minimum time difference is obtained when $r_i = r_j$, and the maximum time difference when either r_i or r_j is 0, so that the causality criterion can be written as:

$$\frac{z_i - z_j}{c} - \frac{R_{ij}}{c}\tan(\theta_c) \leqslant t_i - t_j \leqslant \frac{z_i - z_j}{c} + \frac{R_{ij}}{c}\tan(\theta_c), \quad (4.14)$$

where R_{ij} is the distance between PMT i and j in the plane perpendicular to the muon direction (see also figure 4.1).

The 3N trigger first uses the causality criterion of equation 4.10, where the allowed time difference is increased by 20 ns in order to account for (forward) scattered photons and uncertainties due to calibration. A set of L1 hits that satisfies this causality criterion is called a cluster. When a cluster of at least 5 L1 hits has been found, it is selected for the next step.

The L1 hits in each of the clusters are checked against the directional causality criterion of equation 4.14, where the allowed time difference is again increased by 20 ns. Since the direction of the muon is not known, an isotropic grid of 210 directions is defined on the full sky (with an average spacing between directions of about 14°) and the causality criterion is applied to each of these directions. A sky-map (using azimuth and elevation as coordinates) with the chosen directions is shown in figure 4.2. For the evaluation of the causality criterion, the decreasing intensity of the Čerenkov radiation with distance is taken into account by only using L1 hits with a maximum transverse distance of 90 m. If the cluster still has at least 5 L1 hits (that are compatible with the more stringent directional causality criterion), it is selected.

All selected clusters are saved to disk, together with all L0 hits from 2.2 µs before the first hit to 2.2 µs after the last hit in the selected cluster. A value of 2.2 µs is chosen, since it corresponds to the time a muon needs to traverse the whole detector. The collection of hits is called an *event* and is the input for the reconstruction strategies described in section 4.3.

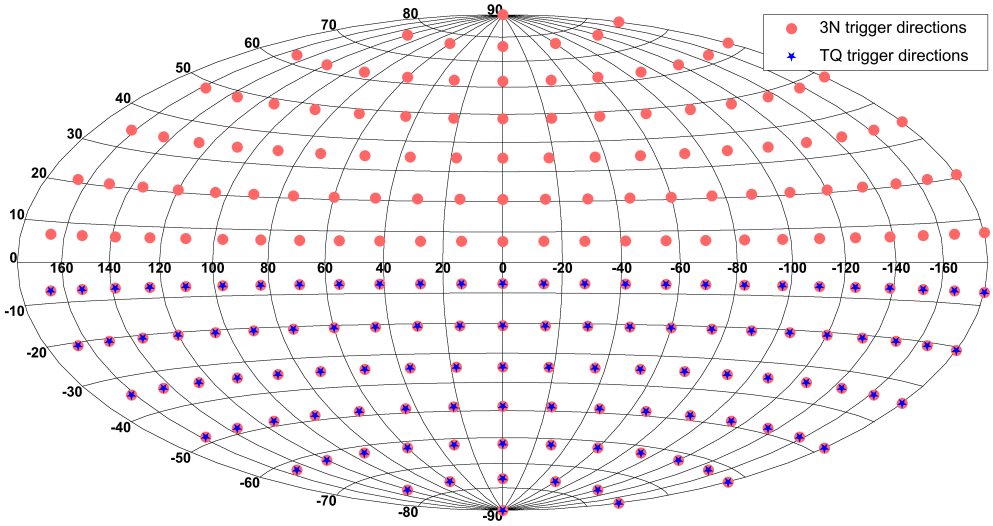

Figure 4.2: Sky-map with the directions used for the directional causality criterion in the 3N trigger and in the TQ trigger.

4.2.2 *The 2T3 trigger algorithm*

The requirement of the 3N trigger to have at least 5 L1 hits in the detector works well for neutrinos of high energy, since the created muon will produce a lot of light, but less so for lower energy neutrinos. For this reason another trigger algorithm has been developed, which is called the 2T3 trigger [Carr et al., 2007]. It is based on the T3 cluster trigger algorithm, which seeks a time coincidence between two L1 hits in adjacent storeys within 100 ns, or in next-to-adjacent storeys within 200 ns. The 2T3 trigger looks for a time coincidence between two of these T3 clusters in the whole detector within 2.2 µs. The algorithm requires a minimum of 3 L1 hits when the two T3 clusters are on the same line and at least 4 L1's otherwise. This gives an improved efficiency for lower energy neutrinos [Escoffier, 2008].

4.2.3 *The directional trigger algorithm*

Besides the general purpose trigger algorithms that look for neutrinos coming from any direction, there are also dedicated directional trigger algorithms. The 1D trigger algorithm uses only L1 hits as input and the mixed (MX) trigger algorithm also uses L0 data.

The directional trigger can be used to track a (hypothesised) neutrino source, which is done by for example the GC trigger which uses the MX trigger algorithm to follow the Galactic Centre. The TQ trigger also uses the MX trigger algorithm, but instead of following a specific source, it uses the directional trigger for a large set of directions. The TQ trigger will be described in the next section.

The first step in the directional trigger algorithms is to check all hits (in the case of the MX trigger L0 and L1) against the directional causality criterion of equation 4.14, for which a prespecified direction is used. The decreasing intensity of the Čerenkov radiation with distance is taken into account again by only considering L0 hits with a maximum transverse distance of 85 m and L1 hits with a maximum of 35 m. The largest set of hits that satisfies the causality relation and includes at least 1 L1 hit is called a cluster. Each cluster which additionally has at least 5 L0 hits is selected.

To reduce the number of accidentally selected clusters, those clusters with at most 10 hits are subjected to a track fit procedure. In general, 5 parameters are needed to parameterise a muon track: the time at a given position along the track, 2 positional parameters and 2 directional parameters. By assuming the muon direction, only 3 parameters are needed, which leads to a linearisation of the track fit problem [de Jong, 2007a]. Using $r_i = \sqrt{(x_i - x_0)^2 + (y_i - y_0)^2}$ and the assumption that $n_g = n$, equation 4.11 can be written as:

$$t_i = t_0 + \frac{z_i}{c} + \tan(\theta_c)\frac{\sqrt{(x_i - x_0)^2 + (y_i - y_0)^2}}{c}, \tag{4.15}$$

and using $t_0^* = t_0\, c / \tan(\theta_c)$ and $t_i^* = t_i\, c / \tan(\theta_c) - z_i / \tan(\theta_c)$:

$$t_i^* - t_0^* = \sqrt{(x_i - x_0)^2 + (y_i - y_0)^2}, \tag{4.16}$$

in which the fit parameter t_0^* appears in a linear way, but the parameters x_0 and y_0 do not. By squaring both sides of equation 4.16 and taking the difference with the same equation for a different hit (j), an equation is found in which all three fit parameters appear in a linear way:

$$(t_j^*)^2 - (t_i^*)^2 - 2(t_j^* - t_i^*)t_0^* = x_j^2 - x_i^2 - 2(x_j - x_i)x_0 + y_j^2 - y_i^2 - 2(y_j - y_i)y_0. \tag{4.17}$$

The problem can thus be formulated in matrix form by considering all pairs of consecutive hits:

$$\mathbb{H}\vec{\theta} = \vec{y}, \tag{4.18}$$

with (for a cluster of n hits):

$$\mathbb{H} = \begin{pmatrix} 2(x_2 - x_1) & 2(y_2 - y_1) & -2(t_2^* - t_1^*) \\ 2(x_3 - x_2) & 2(y_3 - y_2) & -2(t_3^* - t_2^*) \\ \vdots & \vdots & \vdots \\ 2(x_1 - x_n) & 2(y_1 - y_n) & -2(t_1^* - t_n^*) \end{pmatrix}, \tag{4.19}$$

$$\vec{y} = \begin{pmatrix} x_2^2 - x_1^2 + y_2^2 - y_1^2 - (t_2^*)^2 + (t_1^*)^2 \\ x_3^2 - x_2^2 + y_3^2 - y_2^2 - (t_3^*)^2 + (t_2^*)^2 \\ \vdots \\ x_1^2 - x_n^2 + y_1^2 - y_n^2 - (t_1^*)^2 + (t_n^*)^2 \end{pmatrix}, \tag{4.20}$$

$$\vec{\theta} = \begin{pmatrix} x_0 \\ y_0 \\ t_0^* \end{pmatrix}. \tag{4.21}$$

There is no exact analytical solution to equation 4.18, since the system of equations is over-determined (the minimum cluster size is 6). However, the optimal solution can be obtained by minimising the χ^2 given by:

$$\chi^2 = (\vec{y} - \mathbb{H}\vec{\theta})^{\mathrm{T}} \mathbb{V}^{-1} (\vec{y} - \mathbb{H}\vec{\theta}), \tag{4.22}$$

with $\mathbb{V}$ the covariance matrix. It is assumed this matrix is diagonal and that the uncertainties in time and position for each hit are the same. A value of 10 ns is assigned for this uncertainty.

The solution to equation 4.18 is given by:

$$\vec{\theta} = (\mathbb{H}^{\mathrm{T}} \mathbb{V}^{-1} \mathbb{H})^{-1} \mathbb{H}^{\mathrm{T}} \mathbb{V}^{-1} \vec{y}, \tag{4.23}$$

and the quality of the fit can be assessed by calculating the χ^2 probability [Metzger, 2002]. The cluster is selected if this probability is higher than 1%.

To reduce the number of accidental clusters due to the optical background even further, a quantity called the surface density of the hits is used [de Jong, 2007b]. The surface density corresponds to the number of hits per unit area and can be calculated by projecting the hits on the plane perpendicular to the muon track. The hits from the muon are then expected to be concentrated around the muon track, whereas the random background hits will be spread over a larger area.

The surface density is then normalised by dividing by a factor $n_{\min}/(0.25\pi R_{\max}^2)$, where $n_{\min} = 6$ is the minimum number of hits required by the MX trigger (so 1 L1 and 5 L0's) and $R_{\max}$ is equal to the maximum transverse distance considered for L0 hits (85 m). Furthermore this normalised surface density is multiplied by the total charge of all hits, exploiting the fact that optical background hits have on average a lower charge than hits from a muon. The resulting parameter is called ρ. By requiring a ρ value of at least 6 the amount of accidental clusters is reduced by a factor of 100.

Since the MX trigger only requires 1 L1 hit, and in addition at least 5 L0 hits, it is more efficient for low neutrino energies. Compared to the 3N trigger, the effiency is almost a factor of 2 higher at 1 TeV, increasing to a factor of about 20 at 10 GeV [Lim, 2011].

4.2.4 *The TQ trigger algorithm*

The TQ trigger applies the MX trigger to an isotropic grid of 105 directions, which coincide with those directions of the 3N trigger that have a negative elevation, see also figure 4.2. The trigger thus only looks for upgoing neutrino-induced muons and not for downgoing muons. Slightly different parameters are used for the MX trigger in this case. At least 2 L1 hits are required and at least 4 additional L0 hits. Also, the minimum ρ value is slightly relaxed; all clusters with $\rho \geqslant 5$ are kept.

Since the TQ trigger applies the loose MX trigger to 105 directions, the trigger rates will rise fast when the optical background increases and this trigger is thus only enabled when the conditions are favourable (i. e. the optical background rates not too high). This can be seen from figure 4.3 which shows the average base line of the PMT counting rate versus the (data) run number, with the runs for which the TQ trigger was enabled in red. It can be seen that when the rates are too high, which generally happens in spring, the TQ trigger is not enabled.

Data from run number 25682 (taken on January 29th 2007) to run number 68170 (taken on November 30th 2012) are used in this work. The first run coincides with the installation of the fifth detetection line (see section 3.2.2) and is the first data run used for physics analyses. The final run is the last data run used in the data analysis as described in the next chapter.

Calculating the fraction of time the TQ trigger is enabled to the total time the detector is running, shows that the TQ trigger is only enabled for 18.8% of the time. This is not a fair comparison

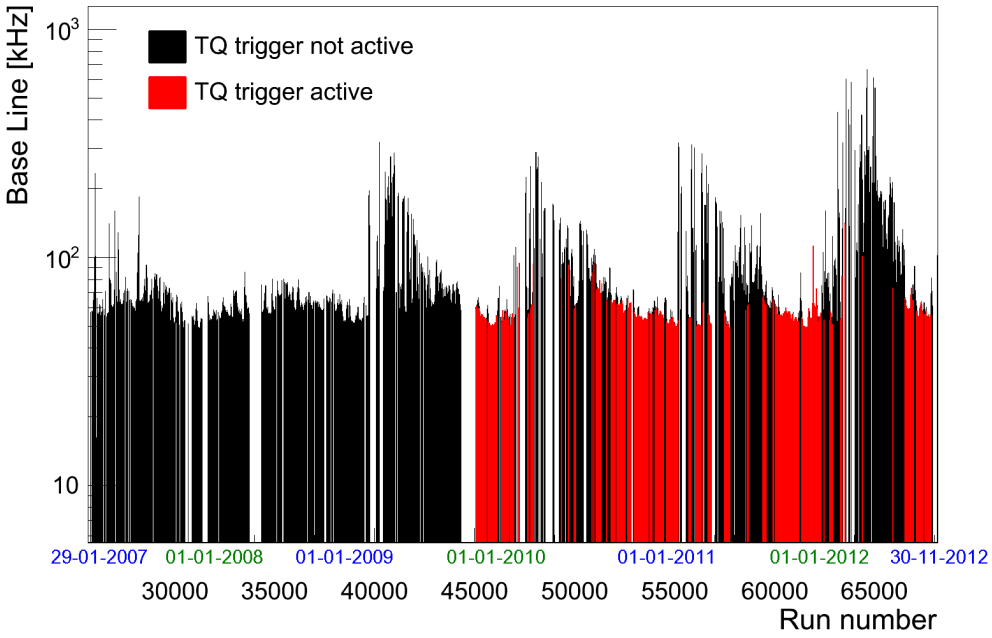

Figure 4.3: The average base line of the PMT counting rate versus data-run number, showing when the TQ trigger is active.

though, since the first data run for which the TQ trigger was available is run 45098, which was taken on December 11th 2009. Recalculating the fraction starting from when the TQ trigger was first available, gives 33.8%.

It should be noted that this fraction could be higher, since there is a subset of runs where the conditions are good, but the TQ trigger has not been enabled. This can be seen from figure 4.4, which shows the distribution of the average base line for all runs in black and those runs for which the TQ trigger is enabled in red, taking only runs after the TQ trigger has first been used. The figure confirms the statement that the TQ trigger is only active when the conditions are favourable; 90% of the TQ trigger runs have an average base line below 60 kHz. However, in only 71% of the total number of runs with an average base line below 60 kHz the TQ trigger has been enabled. If the TQ trigger would have been enabled also in the other 29% of these runs, the trigger would have been active for almost 50% of the total data taking time.

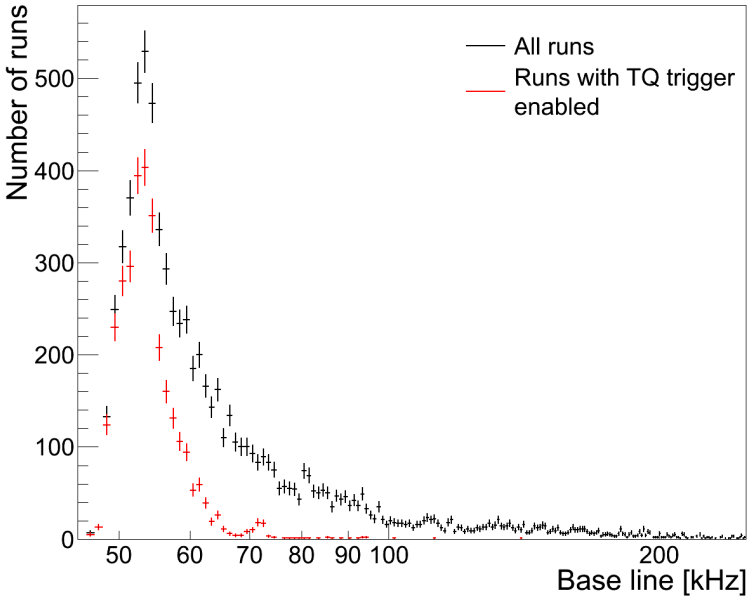

Figure 4.4: Distributions of the average base line.

TQ trigger performance

To quantify the increase in efficiency when using the TQ trigger (compared to the standard 3N and 2T3 triggers), the so-called effective area will be used. The effective area is an important quantity in (neutrino) astronomy and is the area with which the neutrino flux must be multiplied in order to obtain the event rate:

$$R = \int\int \mathrm{d}E_\nu \, \mathrm{d}\Omega \, \Phi_\nu(E_\nu, \theta, \phi) \, A_{\mathrm{eff}}(E_\nu, \theta, \phi), \tag{4.24}$$

with $A_{\mathrm{eff}}(E_\nu, \theta, \phi)$ given by (see equation 4.1):

$$A_{\mathrm{eff}}(E_\nu, \theta, \phi) = \int \mathrm{d}\vec{x} \, \rho(\vec{x}) \, N_{\mathrm{A}} \, \sigma_{\nu\mathrm{N}}(E_\nu) P_\oplus(E_\nu, \theta, \phi) \cdot P_{\mathrm{det}}(E_\nu, \theta, \phi, \vec{x}). \tag{4.25}$$

Using the FXC simulation, the effective area for both the default trigger setup (3N + 2T3 triggers) and for the one with the addition of the TQ trigger (3N + 2T3 + TQ) can be calculated. The effective area as a function of neutrino energy is shown in the left plot of figure 4.5, where the average has been taken for neutrinos and anti-neutrinos. It can be seen that the gain by using the TQ trigger is highest at low neutrino energies, rising to a factor of 2 below

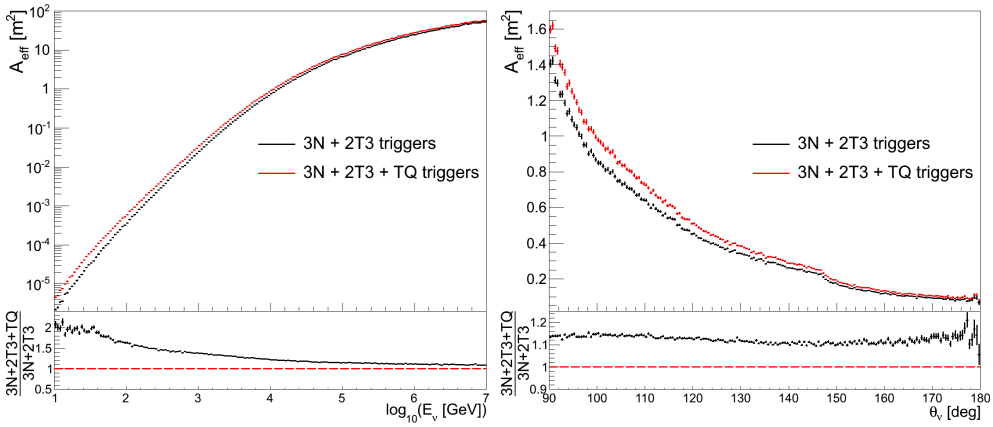

Figure 4.5: Effective area for the default 3N + 2T3 triggers and the default triggers with the TQ trigger added. The average is taken for neutrinos and anti-neutrinos. LEFT: versus energy. RIGHT: versus zenith.

about 30 GeV. Also at higher neutrino energies it is beneficial to use the TQ trigger; the gain being about 20% at 10 TeV.

The right plot in the figure shows the effective areas versus the zenith angle and it can be seen that the total gain by adding the TQ trigger is about 12%, independent of zenith angle.

The gain in terms of event rate depends on the energy spectrum of the neutrinos; the gain will be higher for a softer spectrum than for a harder one, as can be inferred from the left plot of figure 4.5. To quantify this, the cumulative event rates above energies of 100 GeV and 10 TeV are calculated for three different energy spectra: a typical point source spectrum ($\sim E_\nu^{-2}$), the diffuse Galactic spectrum ($\sim E_\nu^{-2.6}$) and the atmospheric neutrino spectrum ($\sim E_\nu^{-3.7}$). Table 4.2 shows the results of these calculations.

ENERGY SPECTRUM	GAIN ABOVE 100 GEV	GAIN ABOVE 10 TEV
Point source ($\sim E_\nu^{-2}$)	21%	16%
Diffuse Galactic ($\sim E_\nu^{-2.6}$)	33%	18%
Atmospheric ($\sim E_\nu^{-3.7}$)	49%	20%

Table 4.2: Gain in terms of event rate by using the 3N + 2T3 + TQ triggers compared to using the default triggers (3N + 2T3).

The gains shown in the table are for when the TQ trigger would be operational 100% of the time. Since the TQ trigger is only active in 18.8% of the runs used for the data analysis, the expected gain in signal for the diffuse Galactic neutrino flux is about 6% when using the TQ trigger. It should be noted however, that the background (atmospheric neutrinos) then also increases by about 9%.

4.3 RECONSTRUCTION

After the trigger algorithms have selected the interesting events, the neutrino direction and energy have to be reconstructed from the hit information. To accomplish this, several reconstruction strategies have been developed which are optimised for a specific neutrino signature.

For neutrino astronomy, the main objective is the reconstruction of the muon direction from the CC interaction of muon neutrinos. Several reconstruction strategies are used in the ANTARES collaboration, of which BBFIT and AAFIT are the most commonly used and are described first in sections 4.3.1 and 4.3.2 respectively. The goal of these reconstruction strategies is to determine the most likely values of the 5 parameters describing the muon track. BBFIT uses a χ^2 approach, while AAFIT maximises a likelihood function.

Within this work, a new track reconstruction strategy has been created, which is optimised to reconstruct low energy neutrinos. This strategy is called GRIDFIT and is described in detail in section 4.3.3. The performance of this new track reconstruction strategy is evaluated by comparing it to AAFIT and BBFIT.

Besides the reconstruction of the direction of the neutrino, the second important parameter that has to be reconstructed is its energy. As discussed in section 2.4.2, the neutrino energy can be used to distinguish the diffuse Galactic signal from the atmospheric neutrino background. The available strategies for the reconstruction of the neutrino energy are described in section 4.3.4.

The reconstruction of NC interactions and of CC electron- and tau-neutrino interactions requires a different approach, since an electromagnetic and/or hadronic shower is created in these interactions, but no muon. The reconstruction of these interactions is called *shower reconstruction*, a brief description of which is given in section 4.3.5.

All plots in this section are based on events which are triggered by the 3N trigger and/or the 2T3 trigger.

4.3.1 *BBFIT*

The BBFIT strategy is developed to provide a fast and robust reconstruction of the muons created in muon-neutrino interactions. BBFIT requires a factor of about 10 less computing time than the full likelihood fit (AAFIT, see next section) [Aguilar et al., 2011c] and is used in online applications like triggering optical follow-up observations or other multi-messenger studies. Since the efficiency for the reconstruction of low energy neutrinos by BBFIT is higher than AAFIT, it is also used for analyses involving, for instance, atmospheric neutrinos [Adrián-Martínez et al., 2012d].

The BBFIT concept is based on the principle that most of the Čerenkov light is seen around the point of closest approach of the muon track to a detector line [Brunner, 2009]. Since the algorithm is designed to run online, the orientations of the OMs are not used. Instead, only time and position information is used, resulting in a simplified geometry. Each storey is considered as a single space point, and hits on OMs on the same storey are combined.

The reconstruction procedure starts with a hit selection; only hits that are selected are used in the subsequent fitting procedure. For the simplified geometry, the hits of the three OMs on a storey are merged if they are closer in time than 20 ns. The time of the earlier hit is taken as the time for the merged hit and the charges of the single hits are added. When hits from different OMs are merged, a bonus charge of 1.5 p.e. is assigned to the merged hit (but only once per merged hit).

Analogously to the L1 hits and T3 clusters used in the triggers, all merged hits with a charge bigger than 2.5 p.e. are called "L1" hits. A "T3" is then defined as the coincidence of two of these "L1" hits within 80 ns for adjacent, and within 160 ns for next-to-adjacent floors (i. e. slightly tighter than used for the 2T3 trigger). Using these "T3" hits as roots, additional hits are searched for in adjacent and next-to-adjacent floors, which are compatible in time with a linear extrapolation of the "T3" hit times along the line. If, for instance, two hits are selected on floors i and $i+1$, with times t_i and t_{i+1} respectively, then the hit time of a hit on floor $i+2$ is assumed to be:

$$t_{i+2} = t_{i+1} + (t_{i+1} - t_i). \tag{4.26}$$

A hit on floor $i+2$ is added to the already selected hits, if it occured in a time window ranging from 10 ns before the time given by equation 4.26 to 10 ns after. If no new hit can be found, neither

in the adjacent nor in the next-to-adjacent floor, the procedure stops and the next "T3" root is considered. Only events with at least 5 hits are selected for the fit.

The hypothesis for the fit is that the selected hits are caused by a muon following a straight trajectory and moving with the speed of light. To build a fit function, three variables have to be calculated. These are the expected arrival time t_{exp} of a Čerenkov photon at a given position along the detector line, its corresponding travel path d_γ and its inclination with respect to the line $\cos\theta_\gamma$. These variables can be calculated from the parameters describing the track, see Aguilar et al. [2011c].

The reconstruction is then based on the minimisation of a quality function given by:

$$Q = \sum_{i=1}^{N_{\mathrm{hit}}} \left[\frac{(t_i - t_{\mathrm{exp}})^2}{\sigma_i^2} + \frac{A(a_i)D(d_\gamma)}{\langle a \rangle d_0} \right], \tag{4.27}$$

which consists of two terms. The standard χ^2 term contains the difference between the measured time of hit i, t_i, and the expected time of this hit, divided by the error on the hit time σ_i. The second term penalises hits with a large charge a_i at large distances from the assumed track. For σ_i a value of 10 ns is taken for hits with a charge higher than 2.5 p.e., and 20 ns otherwise.

The penalty term is not written as a difference between measured and expected amplitude to avoid penalties from hits with a large expected amplitude. Instead, a penalty is given to the combination of high amplitude at large distance, given by the product $A(a_i)D(d_\gamma)$, where:

$$A(a_i) = \frac{a_0 \tilde{a}_i}{\sqrt{a_0^2 + \tilde{a}_i^2}}, \tag{4.28}$$

is the amplitude of the hit corrected for the angular acceptance through:

$$\tilde{a}_i = \frac{2a_i}{\cos\theta_\gamma + 1}, \tag{4.29}$$

and $a_0 = 10$ p.e. is the saturation value, which is obtained when $\tilde{a}_i \gg a_0$. This protects $A(a_i)$ against extreme values of the charge a_i.

A similar method is used for the photon travel distance:

$$D(d_\gamma) = \sqrt{d_1^2 + d_\gamma^2}, \tag{4.30}$$

where $d_1 = 5\,\mathrm{m}$ is the minimum photon travel path, which avoids too strong a pull of the fit to the detector line.

The penalty is divided by the average amplitude $\langle a \rangle$, given by:

$$\langle a \rangle = \frac{1}{N_{\mathrm{hit}}} \sum_{i=1}^{N_{\mathrm{hit}}} \tilde{a}_i, \tag{4.31}$$

to correct for the fact that tracks with a higher energy will produce more light. The factor $d_0 = 50\,\mathrm{m}$ normalises the penalty term and balances it with the χ^2 term.

Depending on the number of lines involved in the hit selection (i. e. the number of lines with at least one "T3"), either a single-line or a multi-line fit procedure is started. For the single-line fits, the azimuth angle of the muon track cannot be determined, since the track geometry is invariant under rotations around the detector line.

When only 2 lines are used for the fit, there always exists an alternative solution that has the same zenith and Q value, but a different azimuth value. To break this degeneracy, a temporary hit selection is performed, where only hits for which the absolute value of the time residual $(t_i - t_{\mathrm{exp}})$ is smaller than 20 ns are selected. The track with the highest weighted charge A_{tot} is then chosen, where:

$$A_{\mathrm{tot}} = \sum_{i=1}^{N_{\mathrm{hit}}} a_i f_{\mathrm{ang}}(\theta_\gamma), \tag{4.32}$$

where $f_{\mathrm{ang}}(\theta_\gamma)$ is the angular acceptance of the PMT, which can be approximated by $\frac{\cos\theta_\gamma + 1}{2}$ (as done in equation 4.29) [Galatà, 2010].

To select well reconstructed events and to discriminate misreconstructed atmospheric muons from neutrinos, the $\tilde{Q}$ parameter can be used, which is defined as:

$$\tilde{Q} = \frac{Q}{N_{\mathrm{dof}}}, \tag{4.33}$$

where N_{dof} is the number of degrees of freedom (the number of hits used in the fit minus the number of fit parameters). Figure 4.6 shows the distribution of $\tilde{Q}$ for both atmospheric neutrinos and misreconstructed atmospheric muons, using only events that are reconstructed as upgoing. It can be seen that by only selecting events with $\tilde{Q} < \tilde{Q}_{\mathrm{cut}}$, a sample can be created of predominantly neutrinos.

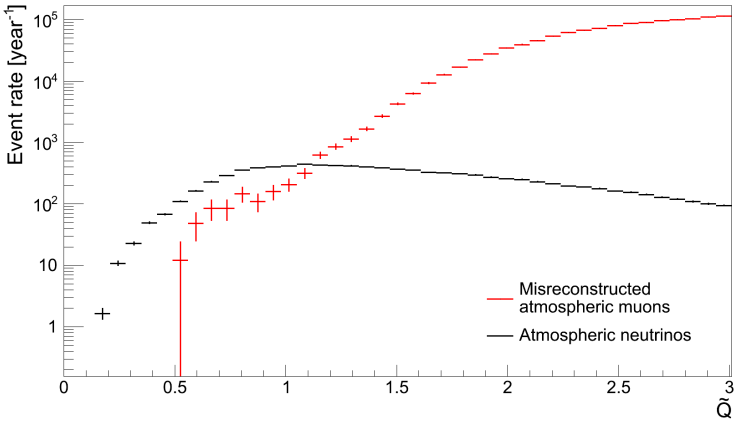

Figure 4.6: Distributions of the $\tilde{Q}$ variable for events reconstructed as upgoing.

To improve the accuracy of the result, an additional fit step is performed for multi-line fits, using the track found by BBFIT as a prefit. A new hit selection is performed, selecting all hits with a time residual smaller than 20 ns with respect to the BBFIT track. These hits are then used to minimise the function:

$$M = \sum_{i=1}^{N_{\text{hit}}} \left[2\sqrt{1 + \frac{(t_i - t_{\text{exp}})^2}{2\sigma^2}} - 2 \right], \tag{4.34}$$

called an M-estimator, which combines the properties of χ^2 and absolute-value minimisation. For small values of the time residual its behaviour is like the χ^2 estimator (see the first term of the sum in equation 4.27), but it becomes linear for large time residuals. This property makes the fit less sensitive to background hits that survive the hit selection, but show large time residuals. For σ a value of 1 ns is chosen, but this value has little impact on the angular resolution [Aguilar et al., 2011c].

The improvement in angular resolution when using the M-estimator can be seen from the distributions shown in figure 4.7. The left plot in the figure shows the distribution of the space-angle error for atmospheric neutrinos. The space-angle error is the angle between the reconstructed (rec) direction and the true (MC) direction of the muon:

$$\begin{aligned}\Delta\alpha \equiv |\alpha_{\text{rec}} - \alpha_{\text{MC}}| = \cos^{-1}(&\sin\theta_{\text{MC}}\cos\phi_{\text{MC}}\sin\theta_{\text{rec}}\cos\phi_{\text{rec}} + \\ &\sin\theta_{\text{MC}}\sin\phi_{\text{MC}}\sin\theta_{\text{rec}}\sin\phi_{\text{rec}} + \cos\theta_{\text{MC}}\cos\theta_{\text{rec}})\end{aligned} \tag{4.35}$$

where θ_i and ϕ_i are the zenith and azimuth of the (reconstructed or MC) track respectively. Only events for which the M-estimator

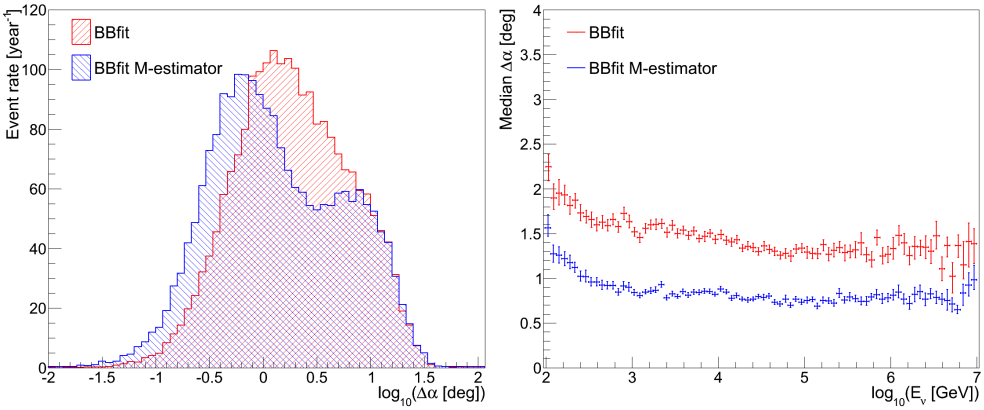

Figure 4.7: LEFT: distributions of the space angle error for atmospheric neutrinos. RIGHT: angular resolution versus neutrino energy.

has been applied (i. e. at least 2 detector lines are used for the reconstruction) are shown in the figure; badly reconstructed tracks are removed by selecting events for which $\tilde{Q} < 1.4$.

The angular resolution is defined as the median of this distribution. The angular resolution is shown versus neutrino energy in the right plot in figure 4.7. Above 1 TeV, the angular resolution is almost independent of energy and improves from about 1.4° for the standard fit to about 0.8° for the M-estimator fit.

Besides a track fit, a bright point fit is also performed, in which the hypothesis of a light source emitting a single flash of light at a given position and time is used. When this fit is applied to hadronic and electromagnetic showers it yields the interaction vertex of the neutrino, see section 4.3.5.

4.3.2 *AAFIT*

The AAFIT reconstruction strategy uses a full likelihood fit to determine the parameters of the muon track and consists of four fit steps [Heijboer, 2004]. The purpose of the first steps is to provide start values for the final likelihood fit that are sufficiently close to the right values.

Like for BBFIT, the reconstruction starts with a hit selection. All hits with an amplitude higher than 3 p.e. and hits in local coincidence are used. A local coincidence is defined as two or more hits on the same storey within 25 ns. Note that this selection

corresponds to the L1 hits, but with a different coincidence time window.

The first fit stage is a linear fit through the positions of the hits. The distance of the muon track to each OM with a hit is estimated using the orientation of the PMT and the amplitude of the hit. It can be expected that an OM recording a high amplitude hit is more likely to be close to the muon track. To obtain a linear relation between the positions of the hits and the track parameters, it is assumed that the hits occur on points along the muon track. The problem can then be formulated in matrix-vector form[20] analogously to equation 4.18:

[20] *Note that the linearisation comes from the assumption that all hits lie on a straight line (the muon track) in this case, while for equation 4.18 the linearisation comes from the assumption on the direction of the muon.*

$$\mathbb{H}\vec{\theta} = \vec{y}, \tag{4.36}$$

with the matrix and vectors given by:

$$\mathbb{H} = \begin{pmatrix} 1 & ct_1 & 0 & 0 & 0 & 0 \\ 0 & 0 & 1 & ct_1 & 0 & 0 \\ 0 & 0 & 0 & 0 & 1 & ct_1 \\ 1 & ct_2 & 0 & 0 & 0 & 0 \\ 0 & 0 & 1 & ct_2 & 0 & 0 \\ 0 & 0 & 0 & 0 & 1 & ct_2 \\ \vdots & \vdots & \vdots & \vdots & \vdots & \vdots \\ 0 & 0 & 0 & 0 & 1 & ct_n \end{pmatrix}, \tag{4.37}$$

$$\vec{y} = (x_1, y_1, z_1, x_2, y_2, z_2, \ldots, z_n)^{\mathrm{T}}, \tag{4.38}$$

$$\vec{\theta} = (p_x, d_x, p_y, d_y, p_z, d_z)^{\mathrm{T}}, \tag{4.39}$$

with p_i and d_i the position and the direction of the track.

The optimal solution to equation 4.36 is given by equation 4.23, which can be found by minimising the χ^2 given by equation 4.22. The covariance matrix contains only the error estimates on the hit positions (which are assumed equal for the x, y and z components); the uncertainties on the hit times are neglected.

The prefit result is only a crude estimate of the track parameters (the median space angle error is about 20°), but it is sufficient as a starting point for the following steps.

To improve the accuracy of the prefit, an M-estimator fit is performed, which is shown to improve the angular resolution (see figure 4.7 for BBFIT). The function that is minimised is:

$$G = \sum_{i=1}^{N_{\text{hit}}} \left[2\kappa \sqrt{1 + a_i (t_i - t_{\text{exp}})^2 / 2} + (1 - \kappa) f_{\text{ang}}(\theta_\gamma) \right], \quad (4.40)$$

where the relative contribution of both terms (the amplitude weighted time residuals and the angular acceptance) is determined by the parameter κ for which the value 0.05 is used.

The sum in equation 4.40 runs over all hits that have a time residual with respect to the prefit between -150 ns and $+150$ ns and are located at most 100 m away from this track. All hits with an amplitude larger than 2.3 p.e. are also selected. The M-estimator fit is only performed when at least 15 hits are selected. The M-estimator greatly improves the angular resolution compared to the prefit; the median space angle error is of the order of a few degrees.

The third step is a Maximum Likelihood (ML) fit, for which the result of the M-estimator fit is used. Hits that have a time residual within[21] $-0.5\,T_{\text{RMS}}$ and $+T_{\text{RMS}}$, where T_{RMS} is the root mean square of the residuals used for the M-estimator fit, are selected; as well as hits with an amplitude above 2.5 p.e. For each set of parameters describing the muon track, the probability to obtain the selected hits can be calculated. This probability is called the likelihood of the event. Assuming the hits are uncorrelated, the likelihood of the event is the product of the likelihood of the hits:

$$L \equiv P(\text{event}|\,\text{track}) = \prod_{i=1}^{N_{\text{hit}}} P(t_i|\,t_{\text{exp}},\, \cos\theta_\gamma,\, d_\gamma,\, a_i), \quad (4.41)$$

in which only the probability of the time of the hits is taken into account. The term in the product is called a PDF.

For the third step a simplified version of the PDF is used, in which the dependence on $\cos\theta_\gamma$, d_γ and a_i is neglected, and the PDF is expressed in terms of only the time residual of the hits. Also the contribution of the optical background hits is not included in this case. The ML estimate of the track is given by the set of track parameters that maximises the likelihood[22].

The last two steps are repeated another 8 times, by rotating and translating the track found by the prefit, to increase the chance of finding the global maximum. Four additional starting points are obtained by rotating the prefit track by 25° around the point on the track closest to the centre of gravity of the hits. By translating

[21] *The interval is not fixed as in the M-estimator hit selection, but rather depends on how close the M-estimator and true tracks are.*

PDF: Probability Density Function

[22] *In practice the maximum value of L is found by minimising $-\log L$, where the logarithm converts the product into a sum.*

the prefit track by $\pm 50\,\mathrm{m}$ in the vertical direction (i. e. straight up and down) and by $\pm 50\,\mathrm{m}$ in the direction perpendicular to both the vertical direction and the direction of the track, four more starting points are obtained. The track with the best reduced likelihood (the likelihood divided by the number of degrees of freedom) is selected as an input for the final reconstruction step. The number of tracks that give the same track direction to within 1° compared to the selected track is called N_{comp} and is used later on for a quality assessment of the track fit.

The track selected in the previous step is used as an input for another ML fit using an improved PDF, which takes the optical background into account and uses the amplitude information of the hits:

$$P(t_i|\, t_{\mathrm{exp}},\, \cos\theta_\gamma,\, d_\gamma,\, a_i) = \frac{1}{N_{\mathrm{tot}}(\cos\theta_\gamma,\, d_\gamma,\, a_i)} \left[P^{\mathrm{sig}}(t_i|\, t_{\mathrm{exp}},\, a_i) N^{\mathrm{sig}}(\cos\theta_\gamma,\, d_\gamma,\, a_i) + R^{\mathrm{bg}}(a_i) \right], \tag{4.42}$$

where $P^{\mathrm{sig}}(t_i|\, t_{\mathrm{exp}},\, a_i)$ is the signal PDF, $N^{\mathrm{sig}}(\cos\theta_\gamma,\, d_\gamma,\, a_i)$ is the expected number of signal hits and $R^{\mathrm{bg}}(a_i)$ is the background rate. The factor $N_{\mathrm{tot}}(\cos\theta_\gamma,\, d_\gamma,\, a_i)$ normalises the PDF and is given by:

$$N_{\mathrm{tot}}(\cos\theta_\gamma,\, d_\gamma,\, a_i) = N^{\mathrm{sig}}(\cos\theta_\gamma,\, d_\gamma,\, a_i) + R^{\mathrm{bg}}(a_i) T, \tag{4.43}$$

where T is the time window in which hits are selected. For the hit selection, all hits with time residuals between $-250\,\mathrm{ns}$ and $+250\,\mathrm{ns}$ with respect to the first ML fit are taken, so $T = 500\,\mathrm{ns}$. All hits with an amplitude larger than 2.5 p.e. are also selected.

Like the $\tilde{Q}$ parameter used in BBFIT to reject the badly reconstructed events, the likelihood of the final ML fit (L^{max}) can be used in AAFIT, since it is expected that events with a higher value of L are better reconstructed. Also N_{comp} can be used, since badly reconstructed events typically have $N_{\mathrm{comp}} = 1$ [Heijboer, 2004]. These two variables are combined to form the Λ-parameter:

$$\Lambda = \frac{\log L^{\mathrm{max}}}{N_{\mathrm{hit}} - 5} + 0.1(N_{\mathrm{comp}} - 1). \tag{4.44}$$

Besides estimates of the track parameters, the fit procedure also provides error estimates. Assuming that the likelihood function follows a Gaussian distribution for all the variables, the (co-)variances can be obtained from the second derivatives of the likelihood function near the maximum. In particular, the esti-

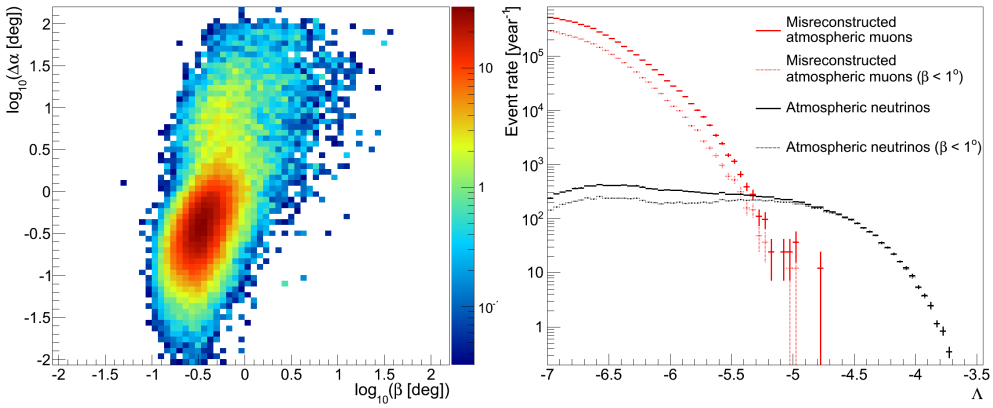

Figure 4.8: LEFT: event rate of atmospheric neutrinos in units of year^{-1} versus β and space angle error, for events with $\Lambda > -5.2$. RIGHT: distributions of the Λ variable for events reconstructed as upgoing.

mated error on the zenith and azimuth angles of the track can be obtained from:

$$\frac{1}{\hat{\sigma}_\theta^2} = -\left.\frac{\partial^2 \log L}{\partial \theta^2}\right|_{L=L^{\max}}, \tag{4.45}$$

$$\frac{1}{\hat{\sigma}_\phi^2} = -\left.\frac{\partial^2 \log L}{\partial \phi^2}\right|_{L=L^{\max}}, \tag{4.46}$$

with the "hat" signifying an estimate[23]. The estimated zenith and azimuth angle errors are combined in the β variable [Heijboer, 2004]:

$$\beta = \sqrt{\sin^2(\hat{\theta})\,\hat{\sigma}_\phi^2 + \hat{\sigma}_\theta^2}, \tag{4.47}$$

which is correlated to the space angle error. This can be seen from the left plot in figure 4.8, which shows the distribution of β versus $\Delta\alpha$ for atmospheric neutrinos, using only events with $\Lambda > -5.2$.

Analogously to figure 4.6 for BBFIT, the distribution of Λ for both atmospheric neutrinos and misreconstructed atmospheric muons, using only events that are reconstructed as upgoing, is shown in the right plot of figure 4.8. It can be seen that Λ can be used to distinguish misreconstructed muons from neutrinos. The β variable can also be used, since applying a cut of $\beta < 1°$ reduces the amount of misreconstructed muons, while the number of well reconstructed neutrinos (i. e. having a high Λ value) is practically unchanged.

[23] *The reconstructed zenith angle is thus denoted by $\hat{\theta}$.*

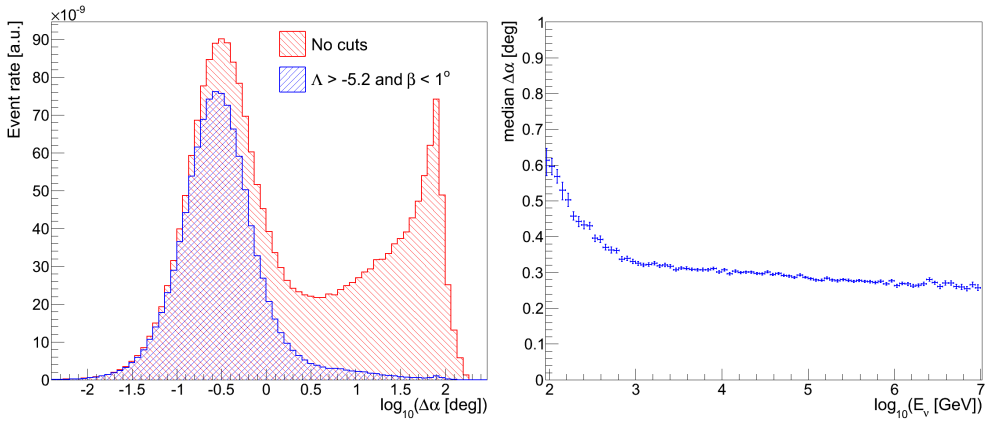

Figure 4.9: LEFT: distributions of the space angle error for E_ν^{-2} neutrinos. RIGHT: angular resolution versus neutrino energy for events passing the point source cuts.

The space angle error distributions are shown in the left plot of figure 4.9. Distributions are shown for all events and events for which $\beta < 1^\circ$ and $\Lambda > -5.2$, which are the cuts applied for the standard point source analysis [Adrián-Martínez et al., 2012a] (which will be referred to as the *point source cuts*). The events are weighted with an E_ν^{-2} spectrum for this figure, since AAFIT is optimised for point source searches for which an E_ν^{-2} spectrum is expected. The angular resolution is shown in the right plot; only for events passing the point source cuts. Above 1 TeV it is nearly independent of energy and is about 0.3°, which corresponds to the intrinsic detector resolution.

4.3.3 *GRIDFIT*

The GRIDFIT strategy is a reconstruction chain developed as part of this work to improve the reconstruction efficiency for low energy neutrinos. Like AAFIT it consists of several fitting steps; three in this case. The first two steps serve to find good starting values of the parameters describing the track, which are necessary for the final likelihood fit. The algorithm will be described first, after which a comparison is made with the existing reconstruction strategies BBFIT and AAFIT.

The algorithm

Like the other reconstruction strategies, also GRIDFIT starts with a hit selection. For GRIDFIT, the Cluster Hit Selection is used [Motz,

2011]. This hit selection is tuned to have a good performance for low energy events. As for the triggers, hits are selected that are close in time and distance. For each hit, a cluster is made of hits that are within a given maximum time and distance window. If the number of hits in such a cluster is larger than a chosen size, the slopes in the $z - t$-plane (with z chosen along the detector line) are calculated between the hit and all other hits that are selected. If the hits are caused by a passing muon, these slopes are expected to be similar (see also [Aguilar et al., 2011c]). Hits for which the slope differs too much from the others are removed until the standard deviation of the slope distribution is below a given value. If the number of hits in the selection is sufficient after the hit removal, the remaining hits are marked for the next step in the hit selection. Besides these hits, hits are also selected if they have a charge larger than a given minimum charge (as is also done in the hit selections for AAFIT and BBFIT).

Three different sub-selections are made, in order to utilise correlations on different scales (see [Motz, 2011] for more details). If a hit is both selected as part of a cluster and exceeds the charge threshold or is selected as part of a cluster in at least two sub-selections, it is selected by the Cluster Hit Selection.

In addition to these hits, all hits are selected that have a charge corresponding to at least 2.5 p.e., which is found to improve the reconstruction accuracy (especially at higher neutrino energies).

After the hit selection, a prefit is performed using the FilteringFit package [Kopper and Samtleben, 2012]. This prefit is based on scanning the whole sky using a given number of isotropically distributed directions. Since a direction is assumed, the track fit problem can be linearised, as is also done for the directional trigger.

The grid of directions is different than that used for the triggers (figure 4.2). It is generated by an algorithm that generates (a, b)-tuples, with $a, b \in [0, 1]$. The zenith and azimuth values are then generated using:

$$\theta = \cos^{-1}(1 - 2a), \tag{4.48}$$

$$\phi = 2\pi b. \tag{4.49}$$

There are different options to generate the (a, b)-tuples, for instance using the scheme from the ANTARES trigger or using a quasi-random generator. Here the (a, b)-tuples are generated by such a generator using the algorithm from Niederreiter [1988]; the other options are found to give comparable results.

For each of the directions a second hit selection is performed using equation 4.14, where the time difference is increased by 5 ns

(as opposed to 20 ns in the trigger) and the maximum transverse distance between the hits is 120 m. The number of hits selected for direction i is called $N_{\text{hits},i}$, which has a minimum value of 4 (since 3 parameters are used for the fitting).

The optimal track is found using equation 4.23 and the χ^2 value is calculated using equation 4.22. For the matrix $\mathbb{H}$ in these equations only the time residuals are used, with the hits ordered in time in such a way as to obtain the largest differences between them. The uncertainty on the hit times is arbitrarily set to 2 ns. The covariance matrix $\mathbb{V}$ is again assumed to be diagonal.

For the FilteringFit prefit 5000 directions are used and the best 9 of these are selected to provide multiple starting points for the final likelihood fit, as is also done in AAFIT. The best directions are selected according to the quality parameter Q:

$$Q = N_{\text{hits}} - w\frac{\chi^2}{N_{\text{hits}} - 3}, \tag{4.50}$$

where w is a weighting factor which determines the relative importance of the number of hits and reduced χ^2 terms. This quality parameter favours solutions which have a large number of clustered hits over solutions with a good reduced χ^2 value, but with a low number of hits. The optimal value of w has been found to be 0.5.

The selection of the best 9 tracks can further be improved by looking at the fraction of hits that can be clustered in the true direction. It has been found that this number is almost always a high fraction of the maximum number of hits found in the grid. At an energy of about 400 GeV, the true direction has at least 80% of the maximum number of hits in ~93% of the events; at an energy of about 200 TeV this is the case in ~80% of the events. So, in the determination of the best 9 tracks, only directions that have at least 80% of the maximum number of hits found are selected.

Since a grid of 5000 directions is used for the prefit, the execution time per event is rather large. It takes on average around 300 ms [Visser and Wagner, 2013] to perform the prefit step per event. For this reason it has been decided to filter out atmospheric muons and only reconstruct those events which are likely neutrino candidates. For this purpose a grid of 500 directions is used to evaluate the GridFit Ratio (R_{GF}) variable, which is defined as:

$$R_{\text{GF}} = \frac{\sum_{\text{UP}} N_{\text{hits},i}}{\sum_{\text{DOWN}} N_{\text{hits},i}}, \tag{4.51}$$

where $\sum_{\text{UP}}$ is performed over all directions with a negative elevation (i. e. directions for which the track is UPgoing) and $\sum_{\text{DOWN}}$ over all directions with a positive elevation.

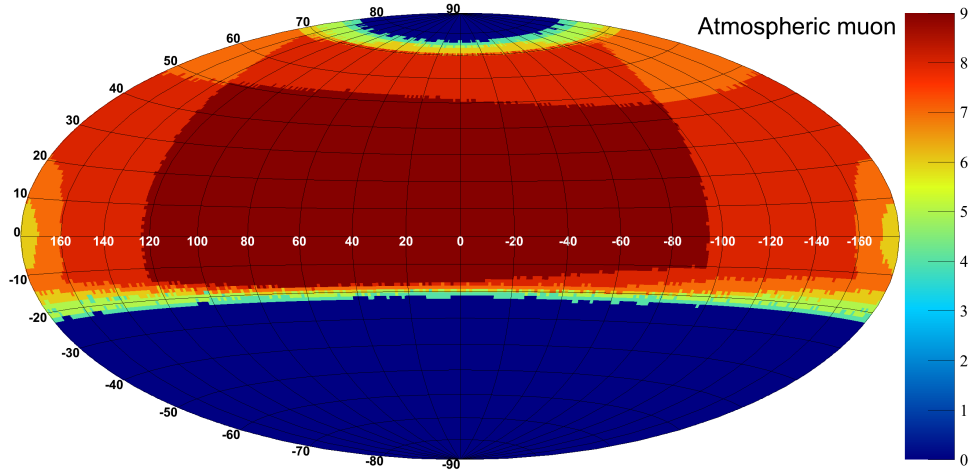

Figure 4.10: Sky-map with the N_{hits} grid for an atmospheric muon.

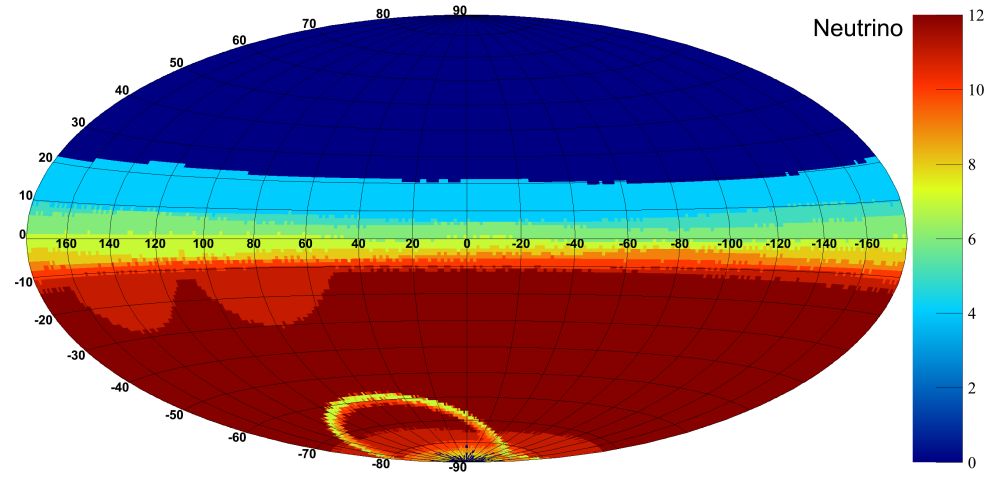

Figure 4.11: Sky-map with the N_{hits} grid for an upgoing neutrino.

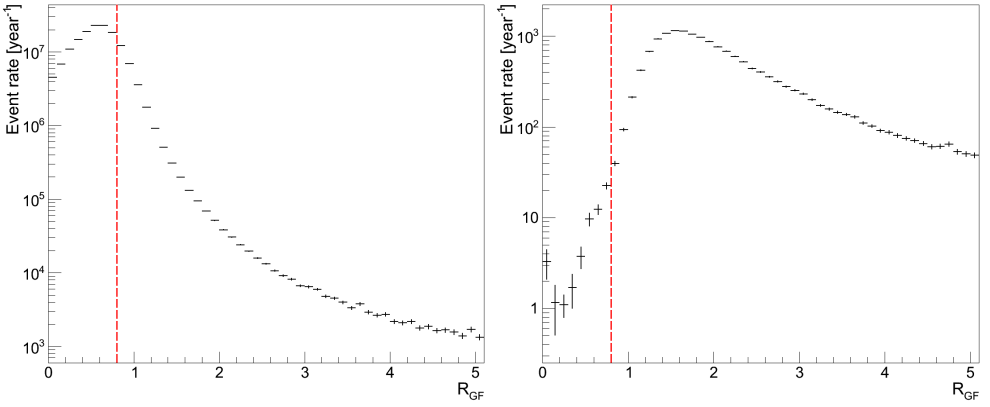

Figure 4.12: Distribution of R_{GF}, the red dashed line indicates the cut value of 0.8. LEFT: for atmospheric muons. RIGHT: for atmospheric neutrinos.

The plots in figures 4.10 and 4.11 show sky-maps of the N_{hits} grid (using azimuth and elevation, as done in figure 4.2) for an atmospheric muon and an upgoing neutrino respectively. It can be seen that for the muon, the number of hits for DOWNgoing directions is higher than for UPgoing directions, which is expected since atmospheric muons are downgoing. For the neutrino it is the other way around; the number of hits for UPgoing directions is higher than for DOWNgoing directions. This information is summarised in the R_{GF} variable: for muons the value is expected to be smaller than 1, while for neutrinos it is expected to be bigger than 1. For the events shown in figures 4.10 and 4.11, $R_{GF} = 0.36$ for the muon and $R_{GF} = 6.77$ for the neutrino.

To filter out atmospheric muons, the R_{GF} variable is used and the reconstruction is performed only for events with $R_{GF} > 0.8$. Figure 4.12 shows the distribution of R_{GF} for both atmospheric muons and neutrinos. The effect of only accepting events with $R_{GF} > 0.8$, is that 81.3% of the atmospheric muons are filtered out and only 0.32% (1.05%) of the atmospheric (E_ν^{-2}) neutrinos.

The angular resolution of the prefits is limited to a couple of degrees, because the points are separated by about 3° in a grid of 5000 points. To improve the angular resolution of this prefit, an M-estimator fit is performed for each of them, as is done in AAFIT and BBFIT. The implementation is identical to the implementation in AAFIT. First a hit selection is performed, selecting all hits that have an absolute time residual smaller than 150 ns with respect to the prefit and are at most 100 m away from it. In addition all hits with an amplitude of at least 2.3 p.e. are

kept. Like in AAFIT, the M-estimator fit is only performed if at least 15 hits are selected.

The effect on the space angle error can be seen from figure 4.13, in which the distribution of the space angle error is shown for the different fit steps. For this, the chosen final track (and corresponding prefit) is used. Since the same M-estimator (and PDF, see below) are used as in AAFIT, the events are again weighted with an E_ν^{-2} spectrum. From the figure it can be seen that using the M-estimator is beneficial, since it improves the angular resolution of the prefit substantially.

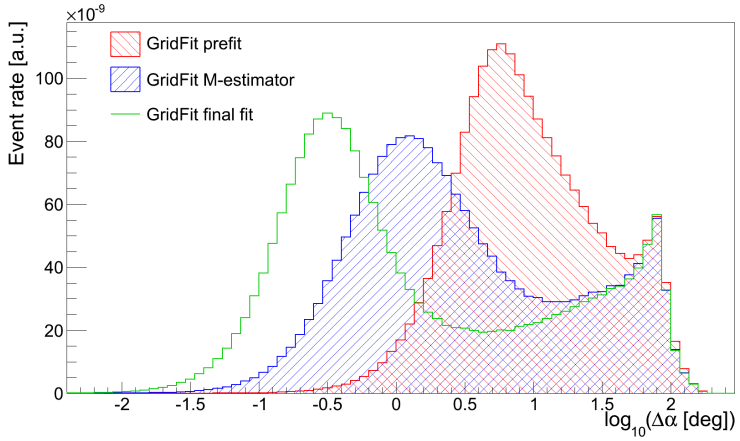

Figure 4.13: Distributions of the space angle error for the chosen final track for E_ν^{-2} neutrinos.

The results of the prefit are used for a final likelihood fit, for which the same PDF is used as in AAFIT (see equation 4.42). It should be noted that only one likelihood fit step is performed here, unlike in AAFIT where two PDF fit steps are performed. In GRIDFIT the first PDF fit step is not performed and the M-estimator results are immediately used for the final likelihood fit. The hit selection is also different than in AAFIT and similar to that of the M-estimator fit. All hits that have an absolute time residual smaller than 150 ns and a maximum distance of 120 m are selected. Since the 9 best tracks from the FilteringFit prefit are chosen, this gives 9 hit selections. These hit selection are merged into one final hit selection. Then, for each prefit the final likelihood fit is performed, using the parameters from the prefit as starting values. The improvement in the space angle error can be seen in figure 4.13.

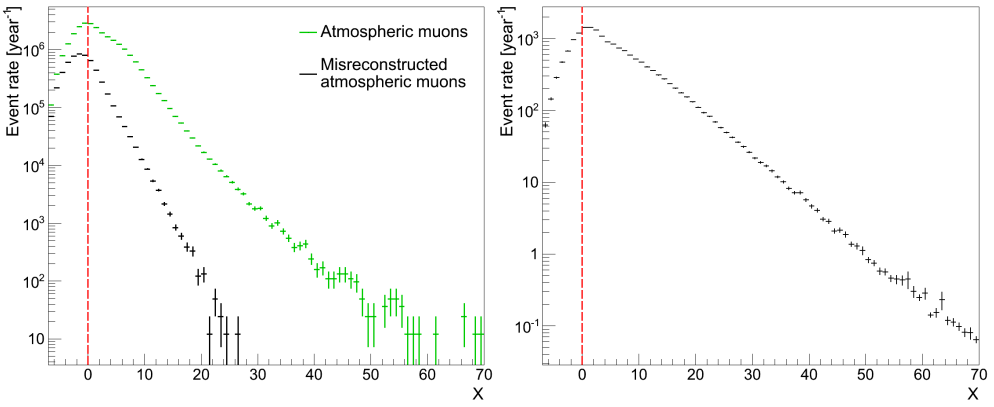

Figure 4.14: Distribution of X, the red dashed line indicates the cut value of 0. LEFT: for atmospheric muons. RIGHT: for atmospheric neutrinos.

Out of the 9 PDF fits, the track with the highest value of X is selected as the final fit result, where X is defined as:

$$X = N_{\text{hits, ff}} + w_x \frac{\log L^{\max}}{N_{\text{hit}} - 5}. \tag{4.52}$$

This selection criterion is similar to the quality parameter Q used in FilteringFit (see equation 4.50) and was found to give good results in selecting the track with the smallest space angle error with respect to the true direction.

Like w in equation 4.50, the weighting factor w_x determines the relative factor between the number of hits close to the final track ($N_{\text{hits, ff}}$) and the reduced log-likelihood (which is the same as in equation 4.44)[24]. The optimal value for the parameter w_x is found to be 1.1, although it should be pointed out that the quality of the reconstruction is stable under small variations [Visser and Wagner, 2013].

[24] *Note that the reduced log-likelihood is negative, hence the '+' in front of the term.*

The number of hits close to the final track in equation 4.52 is determined as follows. Starting with the hits used as input to the final likelihood fits, those hits are selected that have an absolute time residual smaller than 5 ns and a maximum distance of 70 m. This hit selection is very tight and serves to select only those hits that are consistent with the track hypothesis; any background hits that might have been in the hit selection and any hits not consistent with the found track, are thus filtered out.

From equation 4.52 it can be seen that the value of X can become negative. This mostly happens when only a few hits are found to be close to the track. All events for which the value of

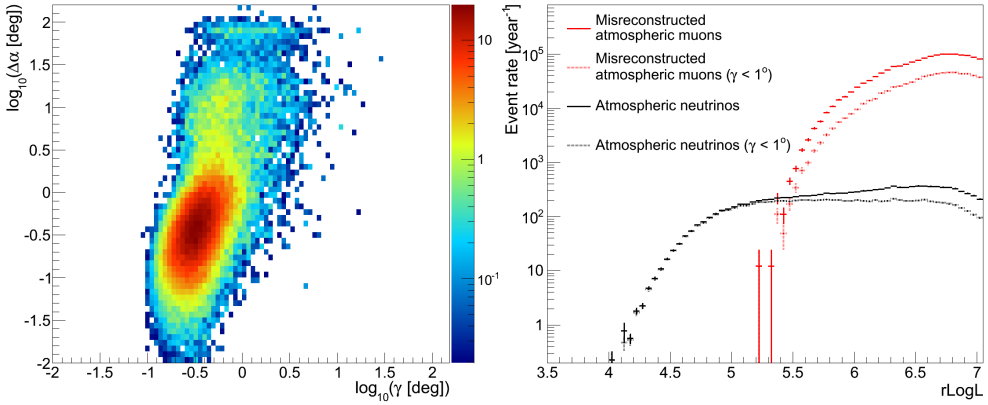

Figure 4.15: LEFT: event rate of atmospheric neutrinos in units of year^{-1} versus γ and space angle error, for events with rLogL > 5.4. RIGHT: distributions of the rLogL variable for events reconstructed as upgoing.

X is negative for all 9 fits, are rejected, since these events were found to be mostly misreconstructed. This can be seen from figure 4.14, which shows the distribution of X for (misreconstructed) atmospheric muons on the left and for atmospheric neutrinos on the right.

By rejecting events with a negative value of X, 22.6% of the atmospheric neutrinos are rejected (4.8% for an E_ν^{-2} flux), 39.0% of the atmospheric muons and 67.2% of the misreconstructed atmospheric muons. It should be pointed out that almost all the events that are rejected by this cut on the X-parameter would also have been cut away when applying quality cuts.

Rejecting misreconstructed muons

Just like the Λ parameter for AAFIT and the $\tilde{Q}$ parameter for BBFIT, the rLogL parameter (which is defined to be minus the reduced log-likelihood from equation 4.52 and so is positive) can be used in GRIDFIT to reject the badly reconstructed events. This can be seen from the right plot in figure 4.15, in which the distribution of rLogL for atmospheric neutrinos and misreconstructed atmospheric muons is shown.

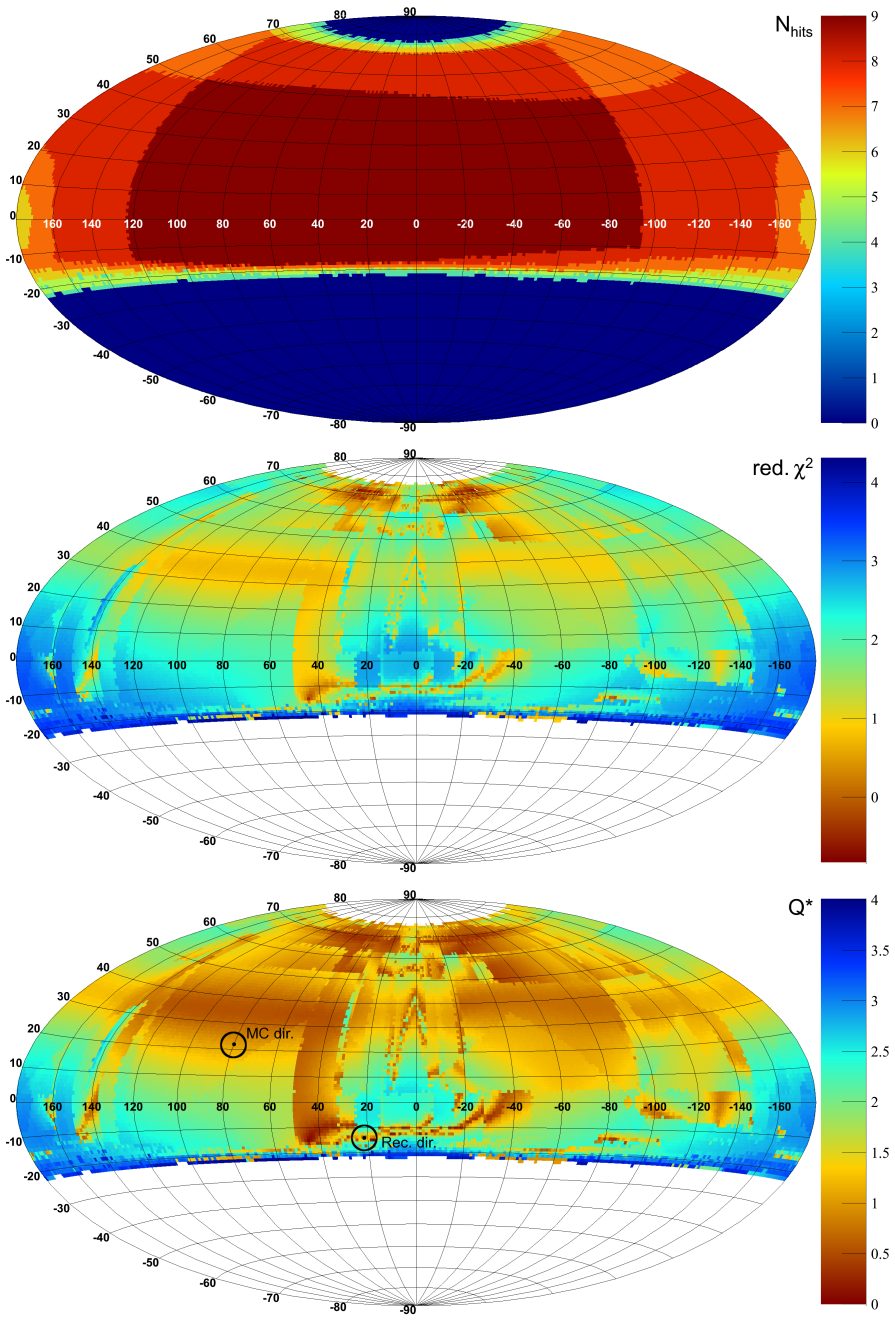

Figure 4.16: Sky-maps for a misreconstructed muon. TOP: N_{hits}. MIDDLE: $\log_{10}$ of the reduced χ^2. BOTTOM: $\log_{10}$ of $Q^* = -Q + C$, where C is the maximum found value of Q plus 1. This is done so that the Q^*-scale always starts at 1.

The estimated error on the zenith and azimuth angles of the track is also calculated in GRIDFIT. Unlike AAFIT this is done by determining the ellipse in the two dimensions of the track directions where the log-likelihood value is 1/2 lower than the found maximum value of the likelihood (which gives the 1σ confidence interval on the directions). This ellipse is determined by defining a new coordinate system, in which the track direction points to the direction with $\theta = 90^\circ$ and $\phi = 0^\circ$, where the distortion of the angles is minimal and the coordinates can be considered Cartesian. Using a Gaussian approximation, the likelihood landscape around the maximum can be considered a paraboloid. The parameters of this paraboloid are fitted using an analytic χ^2 minimisation and used to determine the zenith and azimuth angle errors. See the paper by Neunhöffer [2006] for more information.

The estimated zenith and azimuth angle errors are combined in the γ variable:

$$\gamma = \sqrt{\hat{\sigma}_\phi^2 + \hat{\sigma}_\theta^2}, \tag{4.53}$$

where the fact has been used that the coordinates are almost Cartesian. This variable is very similar to β from AAFIT, and is correlated to the space angle error, as can be seen in the left plot in figure 4.15. For this plot, only events are used for which rLogL > 5.4 (see also the corresponding plot in figure 4.8).

In addition to the rLogL and γ variables, also the R_{GF} variable can be used to reject misreconstructed muons. For this, the same atmospheric muon event as in figure 4.10 is considered. The sky-map of the number of hits found for each direction is shown again in figure 4.16, together with sky-maps of the corresponding reduced χ^2 and Quality grids. Although this is an atmospheric muon event, the reconstructed direction is found in the UPgoing part and the event should thus be classified as misreconstructed. It turns out that, besides filtering out atmospheric muon events, the R_{GF} variable can also be used to reject misreconstructed atmospheric muons. This can also be seen when looking at the distribution of this variable for neutrinos compared to misreconstructed atmospheric muons, which is shown in the left plot of figure 4.17. By taking only events with $R_{\mathrm{GF}} > 1.5$ for instance, 92.2% of the surviving misreconstructed muons is rejected and only 20.0% of the (atmospheric) neutrinos. Note that the R_{GF} variable by itself is not sufficient to get rid of all the misreconstructed muons. It has to be used in combination with the other two parameters (rLogL and γ) described previously.

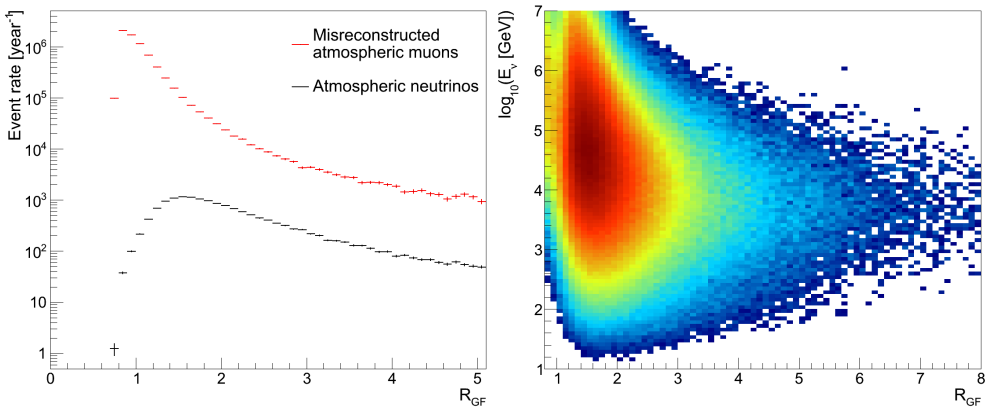

Figure 4.17: LEFT: distributions of R_{GF}. RIGHT: distribution of the event rate of neutrinos (in arbitrary units) versus R_{GF} and neutrino energy.

Although a naive application of R_{GF} works quite well, there is more to gain by looking at its energy and zenith dependence. The right plot in figure 4.17 shows the distribution of R_{GF} versus the true energy of the neutrinos. It can be seen that for higher energies the distribution is more centred around 1.0, while for lower energies there is a large tail towards large values of R_{GF} present. The explanation for this is that the neutrino-induced muons produce more hits at higher energies, so that more hits can be clustered both for upgoing as downgoing directions. Since both the numerator and denominator in equation 4.51 are larger in this case, the value of R_{GF} will be close to 1.0. This effect implies that the R_{GF} variable is not very efficient at high neutrino energies.

To compensate, the cut on R_{GF} can be made dependent on the number of hits used for the final fit, which is a (albeit rudimentary) measure for the energy of the particle in the event. Analogously to how the $\tilde{Q}$ variable of BBFIT is adapted to recover high energy events [Aguilar et al., 2011c], the R_{GF} variable can be adapted as well to make it more efficient for higher energies:

$$R_{\#} = R_{GF} + [0.02 \cdot (N_{\text{hits, ff}} - 5)]^2 , \tag{4.54}$$

for $N_{\text{hits, ff}} > 4$. The effect of this cut can be seen in figure 4.18, in which the event rate distributions versus R_{GF} and $N_{\text{hits, ff}}$ are shown for atmospheric neutrinos and misreconstructed atmospheric muons. For the figure $R_{\#} > R_{\#,\text{cut}} = 1.4$ has been chosen. It can be seen that most of the misreconstructed atmospheric muons are rejected, while most of the neutrino events are kept.

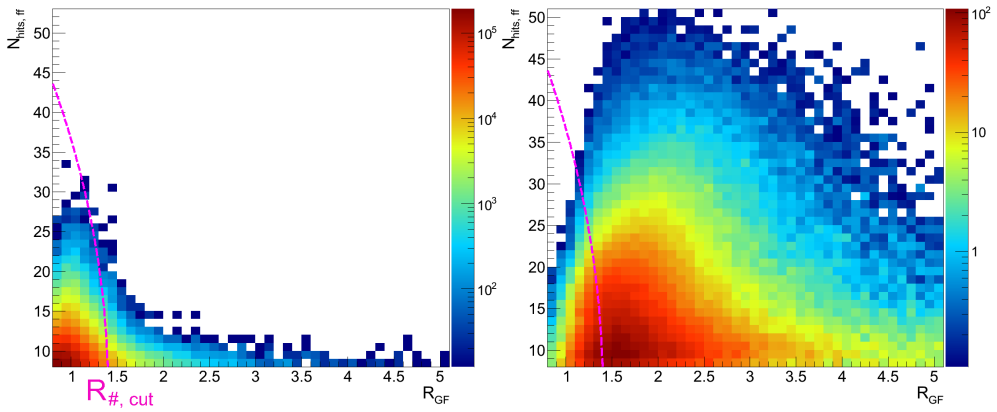

Figure 4.18: Event rate in units of year^{-1} versus R_{GF} and $N_{\text{hits,ff}}$. The purple dashed line represents the cut at $R_{\#} > 1.4$. Note that the colour scales are different for both plots. LEFT: for misreconstructed atmospheric muons. RIGHT: for atmospheric neutrinos.

Figure 4.19 shows the event rate distributions versus R_{GF} and the reconstructed zenith angle. By comparing the left plot (for misreconstructed atmospheric muons) with the right plot (for atmospheric neutrinos), it can be seen that the value of R_{GF} is higher for events that are reconstructed more vertical. This can be understood by the fact that it is more difficult to cluster hits in a downgoing direction if the event is straight upgoing, than it would be when the event would be more horizontal. By adapting the R_{GF} variable, this feature can be utilised:

$$R_\theta = R_{\text{GF}} - R_{\text{diff}} \frac{\hat{\theta}\,[\text{deg}] - 90^\circ}{90^\circ}, \tag{4.55}$$

where R_{diff} determines the slope in the R_{GF}-$\hat{\theta}$-plane. A value of about 1.5 is found to be optimal. Only events with a reconstructed zenith angle of at least 90° are considered, since the focus lies on neutrino events. The effect of adjusting R_{GF} like this is illustrated in figure 4.19, where $R_\theta > R_{\theta,\text{cut}} = 1.0$ has been chosen.

In the following sections, GRIDFIT is compared to BBFIT and AAFIT, and the R_{GF} variable will be used in addition to rLogL and γ to reject misreconstructed atmospheric muons.

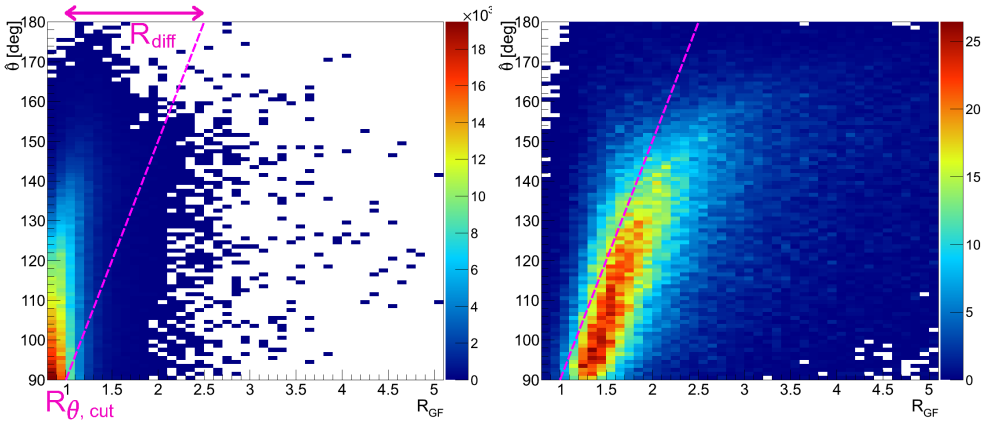

Figure 4.19: Event rate in units of year^{-1} versus R_{GF} and reconstructed zenith angle. The purple dashed line represents the cut at $R_\theta > 1.0$. Note that the colour scales are different for both plots. LEFT: for misreconstructed atmospheric muons. RIGHT: for atmospheric neutrinos.

Comparing reconstruction strategies

In order to compare reconstruction strategies, the cuts on the variables are tuned in such a way as to obtain the same purity. The purity is defined as the percentage of neutrinos in the obtained event sample, which contains both neutrinos (atmospheric neutrinos, neutrinos from for instance point sources, or from some other signal) and atmospheric muons:

$$\mathcal{P} = \frac{N_{\nu_\mu+\overline{\nu}_\mu}}{N_{\nu_\mu+\overline{\nu}_\mu} + N_\mu} \cdot 100\%, \tag{4.56}$$

where $N_{\nu_\mu+\overline{\nu}_\mu}$ is the number of muon-neutrinos plus anti-neutrinos surviving the cuts and N_μ is the number of atmospheric muons surviving. If multiple cut combinations result in the same purity, the combination yielding the largest number of neutrinos is taken.

It is straightforward to obtain the number of atmospheric (anti-) neutrinos from the MC simulation by simply counting the number of events that survive the cuts. Determining the number of atmospheric muons is more tricky, since generally only a few of them will survive the applied cuts. The low statistics of the final sample of atmospheric muons results in a relatively large statistical error. It is also possible that no muon event survives the applied cuts at all. In order to still get an estimate of the number of atmospheric muons and reduce the error in case only a few survive, the following approach is taken. All cuts are applied,

except the cut on the track quality parameter (rLogL for GRIDFIT, $\tilde{Q}$ for BBFIT and Λ for AAFIT). The tail of the cumulative distribution of the track quality parameter is then fitted with an exponential function[25]:

$$N_\mu = 10^{C_1 + q\,C_2}, \tag{4.57}$$

where C_1 and C_2 are fit parameters and q is the track quality parameter. The number of atmospheric muons can then be obtained by inserting the chosen cut value of the track quality parameter in equation 4.57. The error on the number of atmospheric muons can also be determined and is given by:

$$\delta N_\mu = N_\mu \cdot \ln 10 \cdot \sqrt{(\delta C_1)^2 + (q\,\delta C_2)^2 + 2\,\rho\,q\,\delta C_1 \delta C_2}, \tag{4.58}$$

where δC_i is the error on parameter i and ρ is the correlation coefficient, which are all obtained from the fit. Examples can be found in figures 4.20, 4.22 and 4.25.

The strategies are then compared using two figures of merit. These are the effective area (equation 4.25), for which the average is taken for neutrinos and anti-neutrinos and the angular resolution (equation 4.35).

[25] *It should be pointed out that the tail of the distribution can sometimes also be well fitted with a Gaussian function, which falls off faster and would thus result in a lower number of muons. However, the exponential function will give a more conservative result and will always be used.*

Comparison with BBFIT

In the ANTARES collaboration, the BBFIT strategy is used for analyses focusing on low energy neutrinos, such as the neutrino oscillation analysis [Adrián-Martínez et al., 2012d]. The cuts used in the neutrino oscillation analysis are used here for BBFIT, which will be referred to as the *oscillation cuts*:

- $\cos\hat{\theta} < -0.15$
- For single-line events:
  - $N_{\text{hit}} > 7$
  - $\tilde{Q} < 0.95$
- For multi-line events:
  - $N_{\text{hit}} > 5$
  - $\tilde{Q} < 1.3$ (4.59)

Atmospheric neutrinos are used as signal for the oscillation analysis, so all plots in this section are made for atmospheric neutrinos. In the analysis only the standard BBFIT reconstruction is used; the M-estimator fit is not applied.

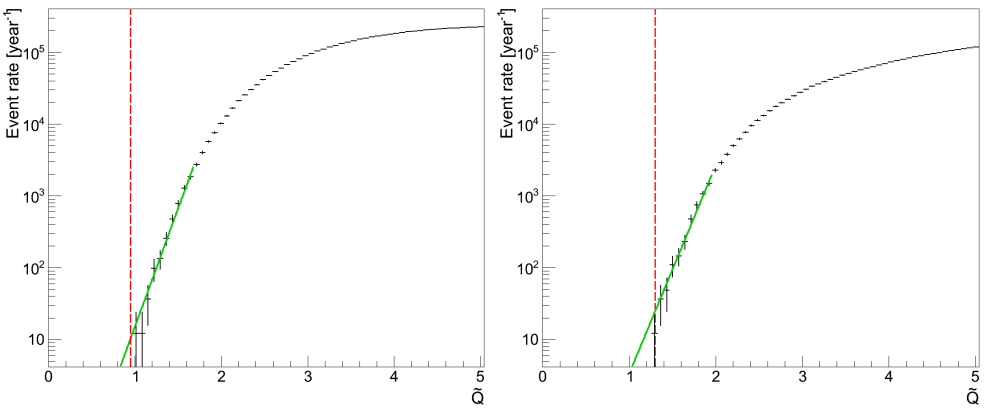

Figure 4.20: Cumulative event rate distribution of the BBFIT $\tilde{Q}$ variable for atmospheric muons. The red dashed line represents the cut. LEFT: for single-line events. RIGHT: for multi-line events.

Using the oscillation cuts, 2110 ± 10 atmospheric neutrinos survive per year (447 ± 7 single-line events and 1660 ± 10 multi-line events). The cumulative muon event rates are shown in figure 4.20. Using the result of the fit, 14 ± 2 single-line events survive per year and 25 ± 5 multi-line events. This gives a purity of $\mathcal{P} = 98.4 \pm 0.3\%$. The effective area is shown in figure 4.21, in which also the contributions of the single-line and multi-line events are shown. It can be seen that the single-line events contribute mostly at low energy, while the multi-line events contribute mostly at high energy.

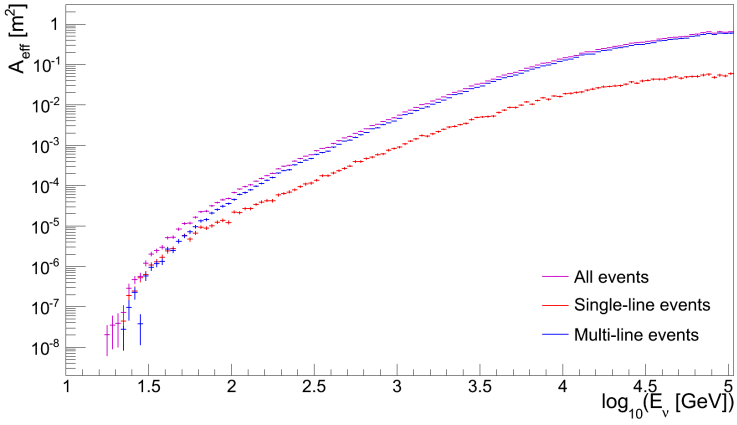

Figure 4.21: Effective area of BBFIT for events passing the oscillation cuts.

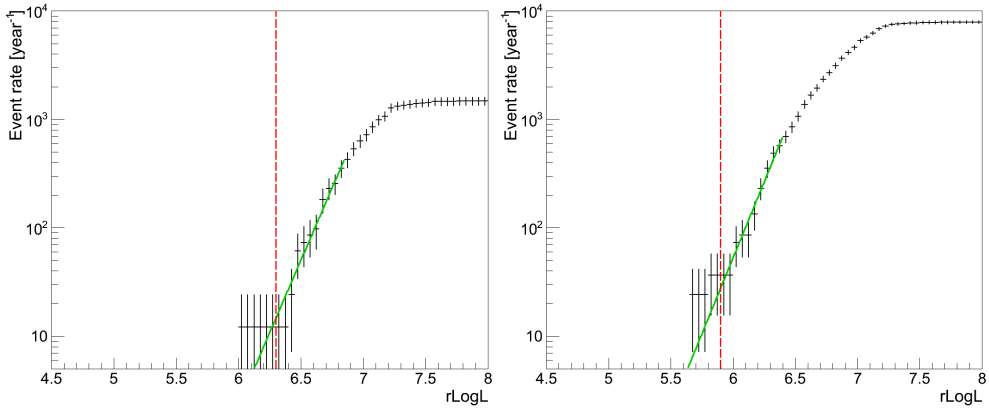

Figure 4.22: Cumulative event rate distribution of the GRIDFIT rLogL variable for atmospheric muons. The red dashed line represents the cut. LEFT: for events passing the Low Energy cuts. RIGHT: for events passing the Recovery cuts.

To obtain the same purity for GRIDFIT and in addition a good efficiency at low energies, a tight cut on R_{GF} will be used, since this variable has been shown to work well for rejecting misreconstructed muons and simultaneously keeping low energy neutrino events. The value of the cut on R_{GF} is varied, after which the rLogL parameter is tuned to obtain a purity similar to BBFIT. It is found that the following cut combination gives good results, which will be referred to as the *Low Energy cuts*:

- $\cos\hat{\theta} < 0$
- rLogL < 6.3
- $\gamma < 20.0^{\circ}$
- $R_{\mathrm{GF}} > 3.5$ (4.60)

As remarked before, the R_{GF} variable works well at low energies, so a tight cut can be placed on it. For low energy events the rLogL value is not that good in general, so it is best to keep this cut as loose as possible. The γ cut is very loose, since the angular resolution is not expected to be important at low energies. Still, this cut is beneficial, since it reduces the amount of misreconstructed atmospheric muons. Applying these cuts, there are 573 ± 9 atmospheric neutrinos surviving per year and 15 ± 2 misreconstructed atmospheric muons (see also the left plot in figure 4.22, in which the cumulative muon event rates are shown for GRIDFIT).

Although the Low Energy cuts work very well at the lowest energies, the efficiency is quite low for higher energy events. This can be seen in figure 4.23, which shows the effective area for events passing the Low Energy cuts in orange. The reason for this is the very strict cut on R_{GF}. To recover the higher energy events, also events passing the following cut combination are kept (this will be referred to as the *Recovery cuts*):

- $\cos\hat{\theta} < 0$
- rLogL < 5.9
- $\gamma < 20.0^{\circ}$
- $R_{\#} > 2.0$ (4.61)

where the value of the cut on rLogL is chosen such that the purity of GRIDFIT is the same as obtained for BBFIT.

This gives an additional 1940 ± 10 atmospheric neutrinos per year and an extra 28 ± 3 misreconstructed atmospheric muons (see also the right plot in figure 4.22). From figure 4.23 it can be seen that this cut does indeed recover the higher energy events.

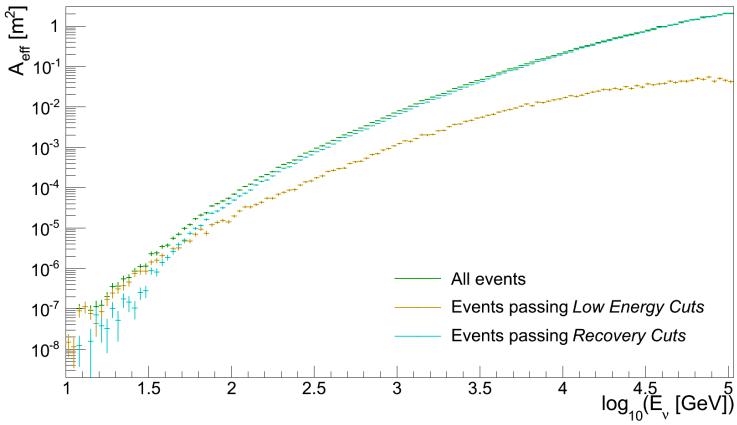

Figure 4.23: Effective area of GRIDFIT for events passing the Low Energy Optimised cuts.

The combination of the Low Energy cuts and the Recovery cuts will be called the *Low Energy Optimised cuts*. For these cuts, the total rate of atmospheric neutrino events is 2510 ± 10 per year and the total rate of misreconstructed atmospheric muons is 43 ± 3 per year. This gives a purity of $\mathcal{P} = 98.3 \pm 0.1\%$. When comparing the number of neutrinos reconstructed by GRIDFIT to the amount reconstructed by BBFIT, it can be seen that GRIDFIT

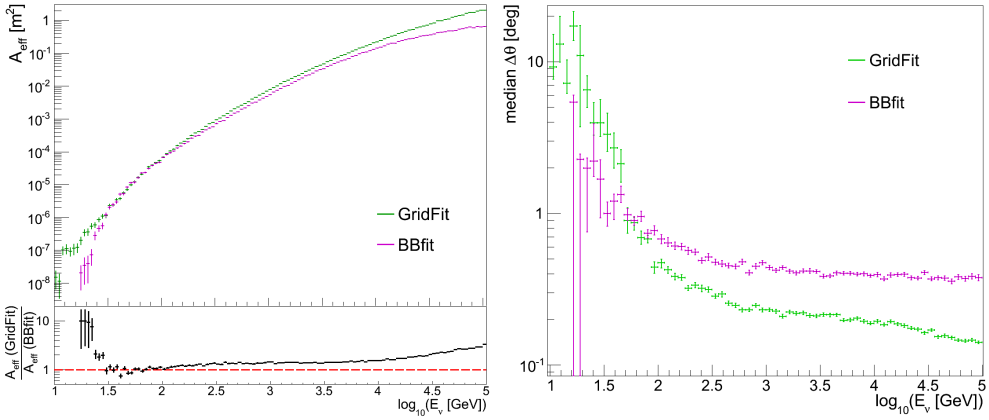

Figure 4.24: Comparison between BBFIT and GRIDFIT. LEFT: effective area versus neutrino energy. RIGHT: zenith resolution versus neutrino energy.

reconstructs almost 20% more neutrinos for the same purity of the final sample.

A more detailed comparison shows that GRIDFIT outperforms BBFIT over almost the whole energy range, with the biggest increase in effective area reached at the lowest energies. It is also important to note that events with energies as low as 10 GeV are reconstructable, although the event rates will of course be limited. This can be seen from the left plot in figure 4.24, which shows the effective areas for both reconstruction strategies together. The effective area of GRIDFIT is comparable to the one for BBFIT in the region from ~35 GeV to ~65 GeV, which is the overlap region of both cut combinations (see also figure 4.23).

The zenith angle resolution[26] is shown for both strategies in the right plot of figure 4.24. For energies above ~50 GeV the zenith resolution of GRIDFIT is better than for BBFIT . For lower energies the zenith resolution of BBFIT is slightly better. The reason for this is the loose cuts on the reconstruction quality and angular resolution estimate, which are required to boost the effiency at these energies. More neutrinos survive in the final event sample, but their direction is not reconstructed as well. It should be noted that the angular resolution is not expected to be important for these low energies. Furthermore, the events reconstructed by GRIDFIT have some azimuth angle information, whereas the single-line events from BBFIT do not. The azimuth resolution is quite poor at the lowest energies, but it is better than a random guess [Visser and Wagner, 2013].

[26] *The zenith angle resolution is compared here instead of the angular resolution, since the single-line events from BBFIT do not have any azimuth information.*

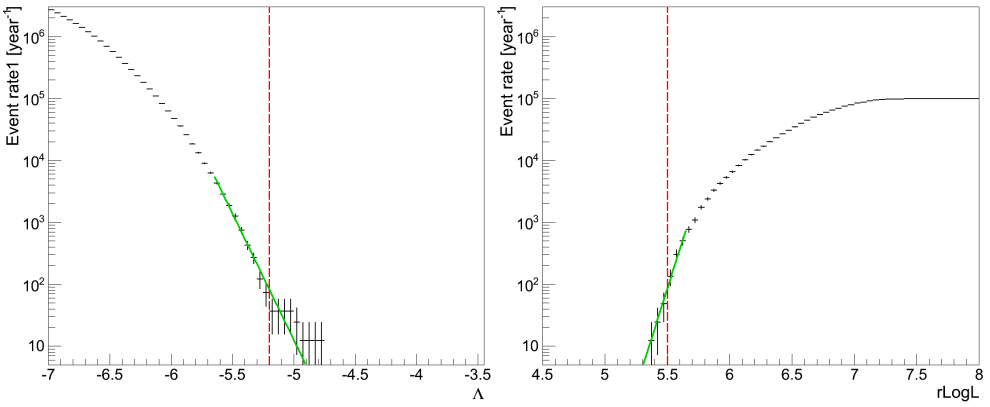

Figure 4.25: Cumulative event rate distribution for atmospheric muons. The red dashed line represents the cut. LEFT: Λ for AAFIT. RIGHT: rLogL for GRIDFIT.

Comparison with AAFIT

Even though GRIDFIT has been optimised for low energies, it is interesting to see how its performance compares to AAFIT. Again, the cuts of both reconstruction strategies are tuned in such a way as to obtain the same purity and after that the effective area and angular resolution are compared.

For AAFIT the point source cuts are used:

- $\cos\hat{\theta} < 0$
- $\Lambda > -5.2$
- $\beta < 1.0^\circ$ (4.62)

In this analysis the assumed signal consists of E_ν^{-2} neutrinos, so all plots are made for neutrinos following this energy spectrum.

Using these cuts 2610 ± 10 atmospheric neutrinos survive per year and 83 ± 9 atmospheric muons, see the left plot in figure 4.25, in which the cumulative muon event rates are shown. This gives a purity of $\mathcal{P} = 96.9 \pm 0.4\%$. The purity obtained here differs from the one given in the paper [Adrián-Martínez et al., 2012a], where it is found to be about 87%. This difference can be explained by the fact that here a perfect detector is considered with 60 kHz background, whereas in the paper more realistic conditions are considered.

To obtain the same purity for GRIDFIT, different combinations of γ and R_{GF} are considered, after which the rLogL cut is tuned in such a way that the purity of GRIDFIT is the same as that ob-

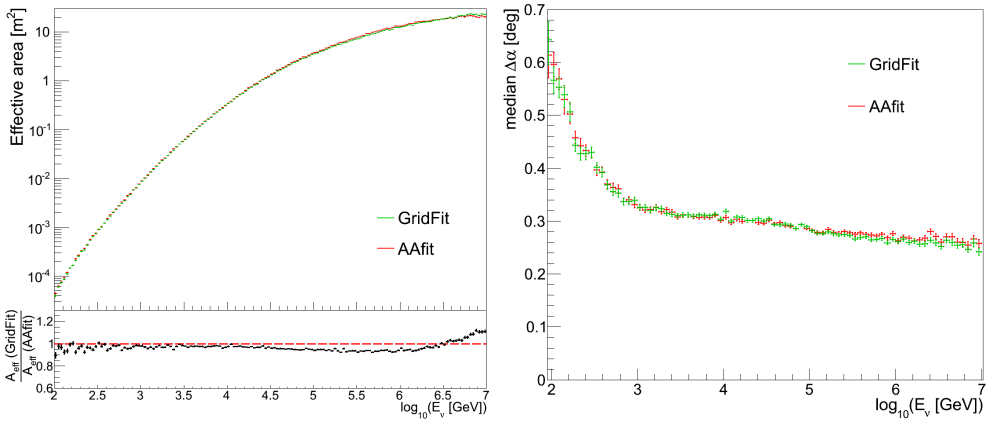

Figure 4.26: Comparison between AAFIT and GRIDFIT. LEFT: effective area versus neutrino energy. RIGHT: angular resolution versus neutrino energy.

tained for AAFIT. In the end it was determined that the following combination gives the best results:

- $\cos\hat{\theta} < 0$
- rLogL < 5.5
- $\gamma < 1.0^{\circ}$
- $R_{\#,\theta} > 0.95$ (4.63)

where R_{GF} is made dependent on both the number of hits used for the final fit and the reconstructed zenith angle (called $R_{\#,\theta}$).

This leaves 2490 ± 10 atmospheric neutrinos and 85 ± 9 misreconstructed atmospheric muons per year (see the right plot in figure 4.25), giving a purity of $\mathcal{P} = 96.7 \pm 0.4\%$.

The left plot in figure 4.26 shows the effective areas for AAFIT (in red) and GRIDFIT (in green). It can be seen that AAFIT and GRIDFIT perform equally well up to 30 TeV; the effective area of AAFIT is about 3% higher. Between 30 TeV and 1.5 PeV the effective area of GRIDFIT is about 7% lower. At the very highest energies, above about 3 PeV, GRIDFIT performs better than AAFIT, yielding an increase in effective area of about 10% at 10 PeV. From the right plot in the figure it can be seen that the angular resolution is essentially the same for both strategies.

It is interesting to point out that not all events found by using GRIDFIT are also found by using AAFIT, and vice versa. For the cut combinations given above, about 7.5% of the triggered events are reconstructed by GRIDFIT and pass the applied cuts, but are not selected by AAFIT. Vice versa, about 9.5% of the triggered

events are selected by AAFIT but not by GRIDFIT. This information could potentially be used to increase the total amount of reconstructed neutrinos or to improve AAFIT, but this possibility has not been pursued any further.

Discussion

GRIDFIT is a reconstruction algorithm with a good efficiency for low energy neutrinos ($\lesssim 100\,\text{GeV}$). The cut combinations can be optimised such that the number of reconstructed neutrinos is increased by about 20% compared to BBFIT, which is the reconstruction algorithm used in current analyses focusing on low energy neutrinos. In addition, GRIDFIT provides some information on the azimuth angle, which is not the case for single-line BBFIT events.

Even though it was set out to be efficient at low energies, the performance at high energies is also good. The efficiency is almost as good as AAFIT in most of the energy range and better than AAFIT for the highest energies ($\gtrsim 3\,\text{PeV}$). The angular resolution is similar to that of AAFIT.

For the analysis of diffuse Galactic neutrinos, which is the focus of this work, the energy range of interest is from about 100 GeV to about 100 TeV, see section 5.4. In this energy range, AAFIT outperforms GRIDFIT by 3% to 7%, so AAFIT will be used as the reconstruction strategy for the analysis.

It has been shown that the R_{GF} variable can be used to distinguish neutrinos from misreconstructed atmospheric muons. The use of this variable is not limited to GRIDFIT and can also be used with other reconstruction strategies. It can be used to increase the efficiency of, for instance, AAFIT, whilst keeping the same purity.

4.3.4 *Energy reconstruction*

After the direction of the neutrino has been reconstructed, there is still one other parameter that has to be determined: the energy. This is the purpose of the energy estimators, for which two basic approaches are used. The energy is either obtained by fitting a distribution of a parameter that is correlated with the energy, or energy-loss patterns are modelled explicitly. The main estimators that are used are the dE/dX estimator, which falls in the former category, and the ANNERGY estimator, which falls in the latter. Besides these two, which will be described in some more detail

ANN: Artificial Neural Network

below, other estimators also exist, see the paper by Schnabel [2013b] for an overview.

As noted previously, the muon loses energy by ionisation and radiative processes when it traverses matter. The ionisation losses are nearly independent of muon energy and can safely be considered a continuous process. The radiative processes cause electromagnetic and hadronic showers along the muon track and are stochastic in nature, so the energy losses are subject to large fluctuations. Above the critical energy, which is several hundred GeV for muons, the radiative processes become dominant and their contribution to the energy loss rises linearly with muon energy. The total energy loss of the muon can be expressed as [Beringer et al., 2012]:

$$-\frac{dE_\mu}{dx} = a(E_\mu) + b(E_\mu)E_\mu, \tag{4.64}$$

with x the amount of matter traversed and $a(E_\mu)$ and $b(E_\mu)$ as in equation 3.5.

From equation 4.64 it can be seen that at low energies, the track length of the muon can be used to get an estimate of its energy. For muons with an energy above the critical energy, the photons produced by the radiative processes can be used for the energy determination. However, due to the stochastic nature, the uncertainty on the energy of the muon is rather large.

The dE/dX estimator [Schüssler, 2012] uses the total number of photons created by the muon to determine its energy loss and from that its energy. The total muon energy loss is approximated by ρ:

$$\frac{dE_\mu}{dx} \approx \rho = \frac{\sum_{i=1}^{N_{\text{hit}}} a_i}{L_\mu \varepsilon}, \tag{4.65}$$

with N_{hit} the number of hits used by the track reconstruction strategy, L_μ the path length of the muon in the detector and ε a factor correcting for the detector efficiency:

$$\varepsilon = \sum_{i=1}^{N_{\text{PMT}}} \frac{e^{-d_i/\lambda_{\text{att}}^{\text{eff}}} f_{\text{ang}}(\theta_{\gamma,i})}{d_i}, \tag{4.66}$$

where the sum runs over all active PMTs and with d_i the distance between the PMT and the reconstructed muon track.

To convert the obtained value of ρ to an energy estimate for the muon, or the neutrino that induced the muon, calibration tables are used that have been created from MC simulations. The

obtained energy resolution is about 0.45 in the logarithm of the energy for well reconstructed muons at 1 TeV energy.

The ANNERGY estimator [Schnabel, 2012] uses a machine learning algorithm to derive the dependence between a set of observables and the energy estimate. In the case of the ANNERGY estimator, an Artifial Neural Network is used, which can be seen as a representation of the PDF describing the relation between the observables and the energy estimate. The list of observables include the number of hits used for the track reconstruction, the total charge of the hits and their average time residual. The obtained energy resolution is just below 0.4 in the logarithm of the energy for well reconstructed muons at 1 TeV energy.

For the analysis of diffuse Galactic neutrinos, the energy reconstructed by the ANNERGY estimator (E_{rec}) will be used to distinguish atmospheric neutrinos and signal neutrinos. The ANNERGY estimator is chosen since the energy resolution is slightly better than that of the dE/dX estimator. It has been verified that using the dE/dX estimator gives comparable results [Visser, 2014].

4.3.5 *Shower reconstruction*

For completeness, some words have to be said about the shower reconstruction strategies. These strategies deal with the reconstruction of the NC interaction of all neutrino flavours, the CC electron-neutrino interactions and most of the tau-neutrino interactions. Instead of a muon, a particle shower is created in these interactions, which is observed as a point source of light.

The first step in the reconstruction is to identify the location of the interaction vertex and the time of the interaction. The bright point fit of BBFIT is one approach used for this, which makes use of a χ^2 fit.

Another shower reconstruction strategy, called DUSJ [Folger, 2013], performs a maximum likelihood fit to determine the vertex time and position. After this step a second maximum likelihood fit is performed, using the information from the vertex fit, to determine the direction and energy of the neutrino that caused the interaction. For the reconstruction of the neutrino direction, it is used that the light is not emitted isotropically, but that the highest light intensity is expected at the Čerenkov angle. The total charge measured by the PMTs can be used to give an estimate of the neutrino energy.